Higher in the mountains: Dynamics of agro-pastoral practices in a low-latitude mountain system (Karkas Mountains, central Iran) during the Mediaeval Warm Period and the Little Ice Age

Morteza Djamali, Emmanuel Gandouin, Arash Sharifi, Philippe Ponel, Kazuyo Tachikawa, Alireza Naqinezhad, Abdolmajid Naderi-Beni, Hamid Lahijani, Jacques-Louis de Beaulieu, Elodie Brisset, et al.

Higher in the mountains: Dynamics of agro-pastoral practices in a low-latitude mountain system (Karkas Mountains, central Iran) during the Mediaeval Warm Period and the Little Ice Age

Morteza Djamali [a,b,*], Emmanuel Gandouin [a], Arash Sharifi [c,d], Philippe Ponel [a], Kazuyo Tachikawa [e], Alireza Naqinezhad [f,g], Abdolmajid Naderi-Beni [h], Hamid Lahijani [h], Jacques-Louis de Beaulieu [a], Elodie Brisset [a,e], Nafiseh Samadi [i], Marjan Mashkour [j], Emma Gamba [a], Dahvya Belkacem [a], Michelle Leydet [a], Alireza Behnam [k], Marta Garcia [e], François Demory [e], Edouard Bard [e]

[a] Institut Méditerranéen de Biodiversité et d'Ecologie, IMBE (Aix Marseille Univ, Avignon Univ, CNRS, IRD), Europole de l'Arbois, 13545, Aix-en-Provence, France
[b] Gobabeb-Namib Research Institute, Walvis Bay, Namibia
[c] Department of Marine Geosciences, Rosenstiel School of Marine, Atmospheric, and Earth Science, University of Miami, Miami, FL, 33149, USA
[d] Beta Analytic Inc., Isobar Science, Miami, FL, USA
[e] Aix Marseille Univ, CNRS, IRD, INRAE, Coll France, CEREGE, Aix-en-Provence, France
[f] Department of Environmental Sciences, College of Science and Engineering, University of Derby, Derby, DE22 3AW, UK
[g] Department of Plant Biology, Faculty of Basic Sciences, University of Mazandaran, Mazandaran, Iran
[h] Iranian National Institute for Oceanography and Atmospheric Sciences (INIOAS), 3 Etemad Zadeh St., Fatemi Ave., 14155-4781, Tehran, Iran
[i] University of Tehran, General Office for developmental Projects and logistics, Tehran, France
[j] Archéozoologie, Archéobotanique (UMR 7209, AASPE), CNRS, Muséum National d'Histoire Naturelle, CP55, 55rue Buffon, 75005, Paris, France
[k] National Iranian Observatory, Institute for Research in Fundamental Sciences, Artesh Highway, Tehran, Iran

ARTICLE INFO

Handling editor: Yan Zhao

Keywords:
Mediaeval Climatic Anomaly
Little Ice Age
Agropastoral activities
Climate impact
Southwest Asia

ABSTRACT

Little is known about the impact of the Mediaeval Warm Period (MWP: 950–1250 CE) and the Little Ice Age (LIA: 1250–1850 CE) on high-altitude agro-pastoral practices and the vertical mobility of human communities in the mountain regions of interior Southwest Asia. Although the area experienced significant socio-political changes during the last millennium, the socio-environmental interactions during these climatic periods remain poorly understood. This study presents a geochronologically well-constrained, multi-proxy geochemical and palaeoecological record from a high-altitude (2500 m) wetland in the Karkas Mountains, located on the central Iranian desert plateau. All proxies, including bioindicators (pollen, non-pollen palynomorphs, fossil insects) and sedimentological and geochemical data (X-ray fluorescence intensity variations, Isothermal Remanent Magnetization measurements, and lithological changes), reveal two contrasting patterns of hydroclimatic conditions and agro-pastoral practices during the MWP and the LIA. Pollen and non-pollen palynomorphs show that the MWP was characterised by intensive cereal cultivation (mainly wheat) and the establishment of permanent agricultural communities, while the LIA was characterised by intensified grazing pressure on montane steppe vegetation, suggesting a shift towards a more mobile pastoral lifestyle—one that persisted into the 20th century. Interestingly, this shift coincides with the Mongol invasion of the Iranian plateau. Variations in lithology, XRF intensities, magnetic field as well as the insect faunal assemblages further provide insights into the wetland hydrological variations and erosional episodes related to land-use and hydroclimatic changes during the MWP and LIA. Based on the Gahak wetland record and regional palaeoclimatic data, we conclude that the MWP in the mountainous areas of central Iran was marked by milder winters and possibly shorter summer droughts, in contrast to the LIA, which had harsher winters and longer-lasting snow cover. Results of the spectral analysis on Gahak record compared to well-known solar cycles, suggest that the climate of the central Iranian highlands is highly sensitive to the variations in solar irradiance. Our findings highlight the significant role of high-altitude

agro-pastoral communities in supplying food to the lowland urban centres of mediaeval Persia, at least during the MWP. Although socio-political changes (e.g. Mongol invasion) could affect the mediaeval societies, the impact of climatic shifts on socio-economic changes should not be underestimated.

1. Introduction

The last two millennia have witnessed frequent climatic fluctuations recorded in both continental and marine archives (McGregor et al., 2015; PAGES2k Consortium, 2017). These fluctuations including the Mediaeval Warm Period (MWP) and the Little Ice Age (LIA) have impacted the annual and seasonal patterns of temperature and precipitation (Büntgen et al., 2016), glacier and snow cover extension (Koch and Clague, 2011; Hughes, 2014; Koch, 2015; Rowan, 2017; Kjær et al., 2022), peat accumulation (Magnan et al., 2018), lake and wetland water levels (Del Socorro Lozano-Garcia et al., 2007), and drought dynamics (Oglesby et al., 2011; Flohr et al., 2017; Fleitmann et al., 2022). They have also impacted human societies by affecting agricultural production (e.g. Pfister, 1981; Pfister and Brázdil, 2006; Peregrine, 2020; Waldinger, 2022). Although there is a consensus on the global nature of these climatic fluctuations, their thermal and hydroclimatic consequences (e.g. glacier mass balance) appear to have varied regionally (Matthews and Briffa, 2005; Ge and Wu, 2011). The social vulnerability to the economic impacts of these hydroclimatic variations could thus have differed even over short geographical distances, as evidenced in central Europe where two adjacent regions with differing social organisations, topographic settings, and microclimatic conditions reacted very differently to the LIA fluctuations (Pfister and Brázdil, 2006). Such spatial variations highlight the need for multiple case studies to understand the spatio-temporal variations in socio-environmental interactions related to these significant Late Holocene climatic phases (Matthews and Briffa, 2005; Pfister and Brázdil, 2006).

In Europe and North America, numerous studies have investigated the effects of the MWP and the LIA on human socio-economy (Thomson and MacDonald, 2020; Waldinger, 2022). However, little is known about the extent of their impacts on societies in the interior Southwest Asia including Iran. Both intervals have left visible ecological and geological fingerprints in various sedimentary archives of the region (Kroonenberg et al., 2007; Ramezani et al., 2008; Djamali et al., 2009; Ramezani, 2013; Leroy et al., 2011; Haghani et al., 2015; Flohr et al., 2017; Bayer Altin and Kayan, 2020). Indeed, the interior of Southwest Asia, including the Iranian plateau, is among the most water-stressed regions of the world (Barlow et al., 2016; Emadodin et al., 2019), where climatic anomalies of the Common Era have reportedly impacted societies throughout history (Büntgen et al., 2016; Gurjazkaite et al., 2018; Fleitmann et al., 2022).

Palaeoenvironmental records from the Iranian plateau suggest that the intensity of anthropogenic activities and their impact on the landscape, water resources, and vegetation markedly increased from the second half of the 1st millennium BCE, with the emergence of imperial powers and the subsequent agricultural and urban development (Jones et al., 2015; Brisset et al., 2019; Saeidi Ghavi Andam et al., 2020; Rashidian and Djamali, 2023; Sharifi et al., 2023). From the 4th millennium BCE, climatic events (such as those around 4.2 ka and 3.2 ka) have been linked to major societal changes, including the decline of the late Bronze Age civilizations in southeastern and northwestern Iran, as well as power transitions between successive geopolitical entities (Sharifi et al., 2015; Gurjazkaite et al., 2018; Vaezi et al., 2022).

Despite the increasing evidence of correlation between climatic events and cultural changes, the natural and documentary archives in this region have not yet been fully explored to investigate the mechanism through which the frequent climate variations, characterized by numerous extreme events, may have affected human socio-economy during times of large-scale migrations, invasions, and conflicts in mediaeval Persia from the end of the Late Antiquity (late 7th century CE).

In this study, we focus on this poorly investigated period by presenting a ca 1500-year long multi-proxy record of geochemical, palynological, and entomological data with a robust chronology from a high-altitude (>2500 m), low-latitude (33°N) mountain site, with the aim of understanding the socio-environmental interactions inferred from variations in the proxy data. Our specific objectives are: (i) to reconstruct the climatic variations of the last two millennia and their impacts on wetland hydrology and sedimentation, (ii) to track vegetation dynamics and floristic changes in the montane steppes surrounding the wetland in response to these climatic variations and the dynamics of agro-pastoral practices, and (iii) to discuss the socio-cultural implications of the reconstructed climatic and ecological changes.

2. Study area

Gahak wetland (33°38′8.31″N; 51°29′50.78″E; 2517 m) is a semi-permanent shallow wetland located in the Karkas Mountains of central Iran (Figs. 1 and 2). Analysis of the Google Earth images show that the wetland has a catchment basin of approximately 21 km^2 and is surrounded by high mountains reaching up to 3224 m (Mt Kolah Barfi) and receives water from snowmelt, run-off, and numerous small springs. Traces of a qanat system can be identified at the western end of the wetland (Fig. 2B). The wetland's surface area can vary substantially on a seasonal and inter-annual basis depending on the amount of annual precipitation. For instance, in July 2018, a maximum extension of 0.31 km^2 was observed, while in September 2009, a minimum extension of 0.04 km^2 could be estimated based on Google Earth data. The wettest part of the wetland, in the east, is waterlogged almost all year.

2.1. Climate

Gahak is close to the meteorological station of the mountain village of Abyaneh (Fig. 1, lower right panel) with 213 mm/yr and 11.9 °C of annual precipitation and mean annual temperature, respectively. Although located at high elevations (>2500 m), the dry season lasts for six months from May to October. Four months of the year (December to March) experience frosts. The peak of precipitation happens in late winter, early spring. There is a steep climatic gradient from the high mountains to the desert environments surrounding Karkas Mts. In Kashan (Fig. 1, lower left panel), the duration of dry season increases to eight months, annual temperature goes up to 19.1 °C and annual precipitation is 138 mm/yr far below the defining limits of a true desert environment (Quinn, 2009). In Global Bioclimatic Classification system, Kashan falls within Mediterranean desertic-continental while the high mountain areas of Karkas display a Mediterranean xeric to pluviseasonal-continental bioclimate with shorter dry seasons (Djamali et al., 2011).

2.2. Vegetation

The upland vegetation at elevations between 2000 and 3500 m is characterised by a typical species-rich Irano-Turanian montane steppe dominated by *Artemisia* cf. *aucheri*, *Cousinia* spp., *Euphorbia* spp., *Bromus* spp., *Stipa turkestanika, Eryngium* sp., *Astragalus* spp., *Acantholimon* sp., *Acanthophyllum* sp., *Achillea* sp., and *Echinops* sp. (Fig. 3). Submitted to increasing grazing pressure at lower elevations, *Astragalus* spp. become the dominant plant and together with *Artemisia aucheri* form a community. Some large and old trees are cultivated including *Populus* and *Salix* whose timber are found in the ruins of unknown-age stone

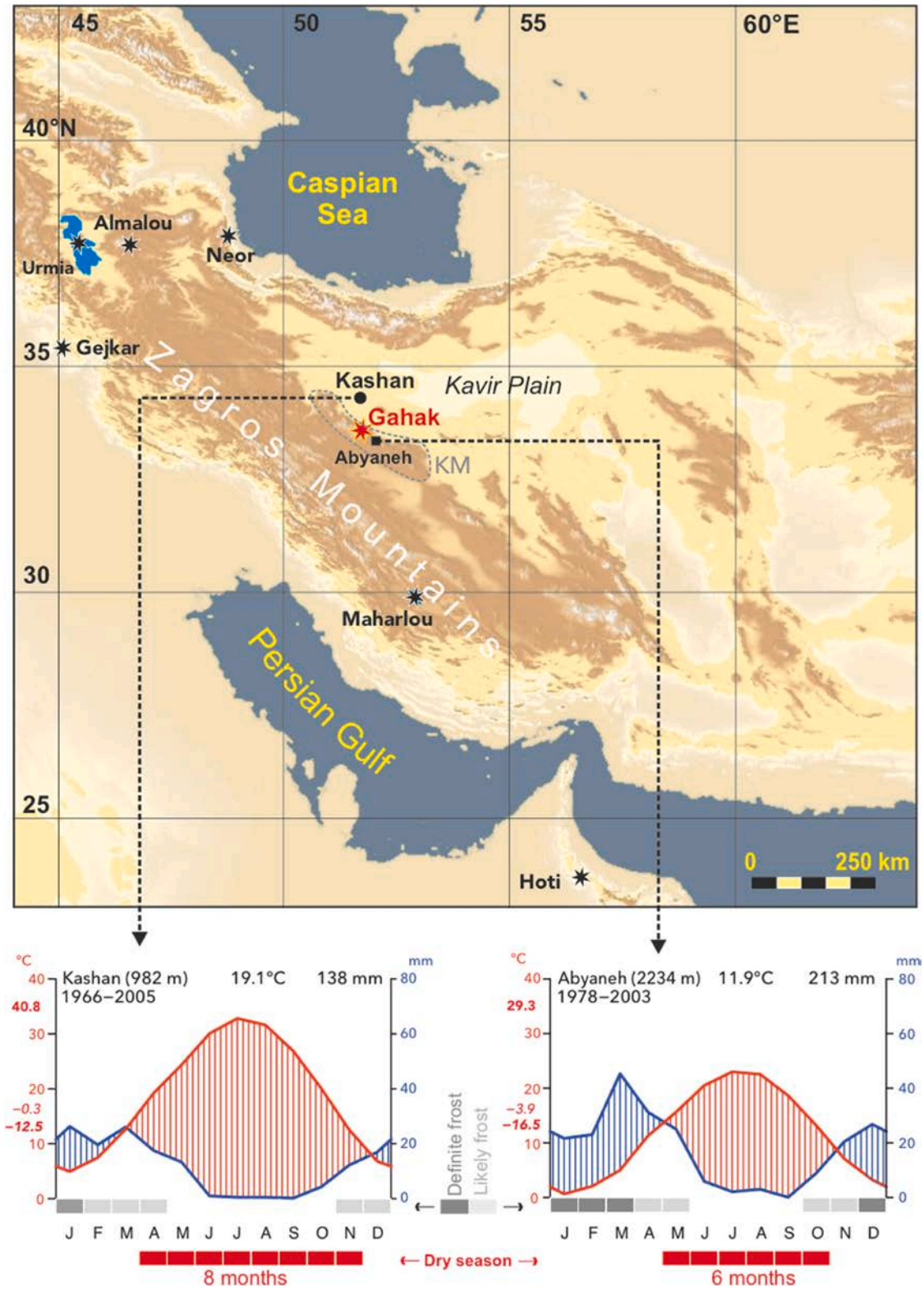

Fig. 1. Location of Gahak wetland in the Karkas Mountains (gray dotted line "KM") in western central Iranian plateau is marked with a red star. Black stars denote the regional palaeoclimate records referred to in this study. Climate diagrams of the city of Kashan in the desert and the Abyaneh village in the mountain (data from the Iran Meteorological Organization, www.imo.ir) show marked changes in annual/seasonal precipitation and temperature as well as the duration of dry season along the desert-mountain gradient. Red horizontal bars show the number of dry months (8 for Kashan and 6 for Abyaneh). Temperature values in bold to the top-left of the diagrams correspond to the mean of the maxima of warmest month of the year. Temperatures to the bottom-left of the diagrams represent the absolute minimum temperature of the whole period (bold italic) and mean of the minima of coldest month (narrow italic). (For interpretation of the references to color in this figure legend, the reader is referred to the Web version of this article.)

buildings around the wetland.

Based on our field observations, three vegetation zones could be respectively distinguished within the Gahak wetland which is indeed a mountain fen: open permanently-waterlogged zone (easternmost corner of the wetland), semi-permanently wet peatlands, and seasonally flooded peripheral zone. The open waters of the eastern part of the wetland are covered by emergent *Phragmites australis*, *Ranunculus trichophyllus*, *Zannichellia palustris*, and *Chara* sp. The peat surface is mainly dominated by *Carex orbicularis, Trifolium pratense, Agrostis stolonifera, Blysmus compressus, Pedicularis sibthorpii, Dactylorhiza umbrosa, Festuca rubra, Poa pratensis, Eleocharis* spp., *Cirsium* sp., *Triglochin palustris*, *Juncus gerardii*, *Plantago maritima*, *Plantago lanceolata*, and *Scorzonera* sp. In the hygromorphic soils close to the surrounding upland dry steppes, the following plants are frequently observed on the peripheral zone: *Hordeum* cf. *violaceum*, *Plantago maritima*, *Mentha longifolia*, *Glaux maritima*, *Trichophorum pumilum*, *Medicago* spp., *Bolboschoenus affinis*, *Alopecurus pratensis*, *Juncus* spp., and *Carex songorica*. The latter zone is currently (July 2018) overgrazed and it is expected that livestock grazing will advance to the peatland at the end of the dry season.

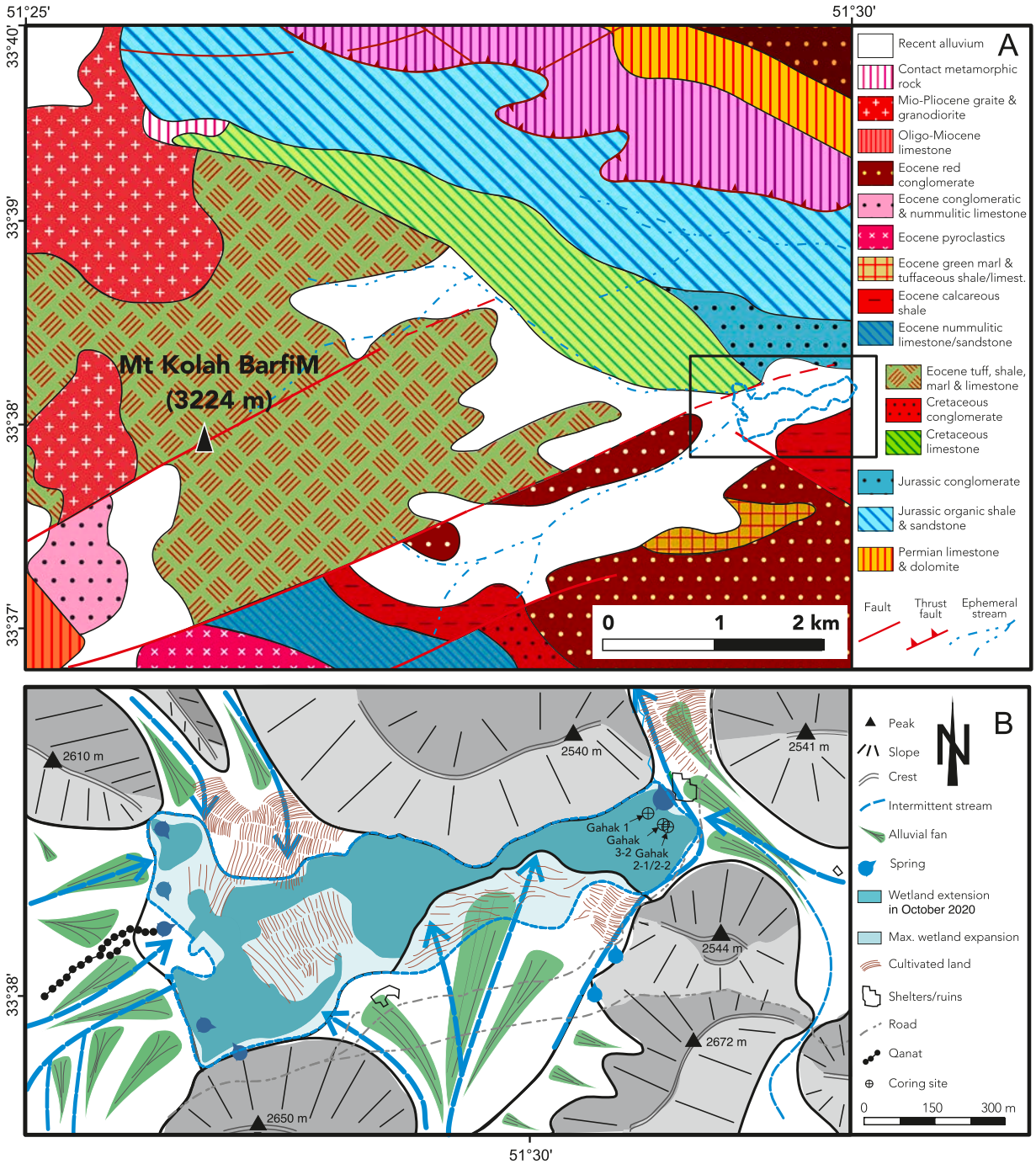

Fig. 2. Geological (A) and geomorphological (B) maps for Gahak wetland area with the location of the coring site. Panel B is a zoom on the inset rectangle to the right of panel A. Geology map is based on the 1:100.000 geological map of Kashan (Radfar, 1993). Geomorphological map is based on satellite image interpretation (Google Earth) and field observations.

2.3. Geology

The study area is located in the Karkas Mountain range and is structurally part of the Sanandaj-Sirjan and Urumia-Bazman magmatic belts. It is significantly deformed by the Main Zagros Thrust Fault. Most of the sedimentary rocks in the area are in fault contact with Cenozoic magmatic rocks due to this extensive deformation (Stöcklin, 1968; Amidi, 1977; Berberian and King, 1981; Isfahani and Sharifi, 1999; Hassanzadeh and Wernicke, 2016).

The geology of the Gahak drainage basin is dominated by both carbonate and siliciclastic rocks ranging from Triassic to Tertiary (Fig. 2A). The immediate slopes have outcrops composed of Jurassic to Cretaceous conglomerates, sandstones and limestones. However, the Eocene volcaniclastics (andesites and tuffs) constitute the largest surface outcrops of geological formations in the catchment (Radfar, 1993).

2.4. Agro-pastoral practices

Today, the wetland surroundings form the summer highland pasture ('yaylak') for the semi-nomadic people of Kashan area who practice transhumance and high elevation agro-pastoralism during the summer months. The grazing of highland pastures by livestock (sheep and goat) starts from April to October when the mobile agro-pastoral communities of Kashan suburbs are present on the site. No rain-fed wheat farming is currently practiced because of the insufficient spring rainfall. The winter wheat is sown in October–November and the germinated plants are left the whole winter covered under snow for several months. The wheat fields need to be irrigated three or four times in late spring and early summer to compensate for the long dry season of the area lasting six months (Fig. 1). The wheat grains are harvested from August to September. In late spring and summer, many vegetables including eggplants, cucumber, and tomatoes are also cultivated and irrigated using water from the wetland and surrounding springs.

3. Materials and methods

3.1. Field works

Three sediment cores were extracted with stratigraphy intact using a Russian peat borer. They were labeled Gahak 1, Gahak 2, and Gahak 3 (Fig. 2B). Gahak 1 was not studied due to incomplete recovery. We selected the most completely retrieved sister core sections of Gahak 2 (two drives labeled 2-1 and 2-2) and Gahak 3 (one drive labeled 3-2) to create a composite section of 120 cm in length (hereafter referred to as Gahak 2–3) which we analyzed in this study (Fig. 4). The cores were taken from the peat surface in the eastern part of the wetland which remains wet most of the year (Fig. 2B). A red soil horizon located at 120–130 cm (core section 2-2 in Fig. 4) marked the base of all cores and possibly the beginning of wetland sedimentation. The cores were sealed in non-reactive plastic sheets, placed within halved PVC core liners and stored in a cold chamber. In July 2018, a botanical excursion/survey was also conducted around the Gahak wetland to prepare a checklist of main aquatic and semi-aquatic plants colonizing the wetland and its peripheral area.

3.2. X-ray fluorescence (XRF) and magnetic core scanning

The Gahak 2–3 composite section was subsampled longitudinally by U-channels with a 20 mm × 20 mm cross-sectional area. A high-resolution, non-destructive XRF core scanning was performed at 5-mm resolution using an ITRAX scanner (Cox Analytical Systems; Croudace et al., 2006) to measure the relative abundance of Si, K, Ca, Ti, Mn, Fe, Rb, Sr, Zr, and incoherent/coherent scattering ratio (hereafter inc/coh, indicator of organic matter and pore water content). The Mo tube was used as an X-ray source at 30 kV, 45 mA with 15 s of counting. The U-channels were then scanned with a recently-developed high-resolution magnetic scanner to measure the magnetic field variations induced by artificially-induced isothermal remanent magnetization (IRM) (Demory et al., 2019). This new technique is more performant in detecting more subtle changes in magnetic properties of sediments compared to the commonly measured magnetic susceptibility. XRF measurements were performed at Inorganic Geochemistry Unit and IRM magnetic field measurements were performed at Rock Magnetic Laboratory at CEREGE (Aix-en-Provence, France).

3.3. Chronology

A total of seven samples (3 peat and 4 organic mud) were selected along the core and sent to Poznan Radiocarbon Laboratory for ^{14}C analysis. Ages and their associated errors were calibrated using IntCal20 calibration dataset (Reimer et al., 2020) in OxCal version 4.4 program (Bronk Ramsey, 1995) and age-depth models were established using both 'clam' and 'Bchron' R packages (Blaauw, 2010; Parnell et al., 2008). Ages and their associated uncertainties were reported in 2-sigma ranges in calendar years after Common Era (cal yr CE). One exception is however, the youngest age which is reported as post-bomb concentration expressed in percent Modern Carbon (127.63 ± 0.37 pMC) and was calibrated using the post-bomb NH2 calibration curve in OxCal (Hua et al., 2022; Reimer et al., 2020). To calculate the possible age offset caused by 'reservoir effect', we dated a new sample at 71–72 cm depth close to a bulk sample at 72–74 (Table 1). This sample was dated using AixMICADAS system at CEREGE, Aix-en-Provence, France (Bard et al., 2015; Tuna et al., 2018).

Fig. 3. Gahak wetland photographed in Spring (2018) as viewed from the North. Coring site is located in the water-logged area to the left of the photo (arrow).

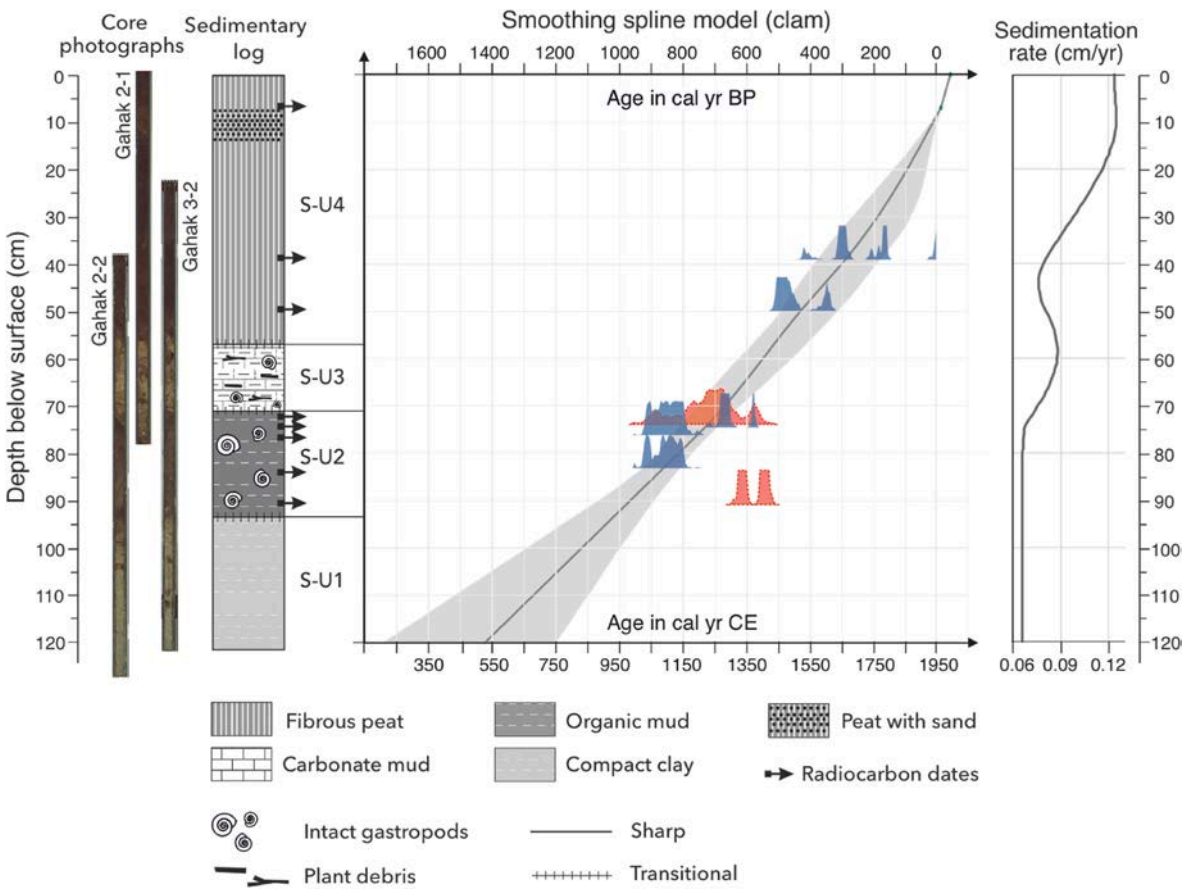

Fig. 4. Sedimentary log and age-depth model of Gahak 2–3 sediment core. The excluded ages are colored in red and bordered by a dash line. (For interpretation of the references to color in this figure legend, the reader is referred to the Web version of this article.)

Table 1
Radiocarbon age results. Please note that unlike all other ages which are reported as ^{14}C ages in yr BP, the most recent age is reported as post-bomb concentration expressed in percent Modern Carbon (127.63 ± 0.37 pMC). Calibrated age uncertainties are reported in 2-σ range. Calibrations were performed in OxCal 4.4 (Bronk Ramsey, 1995) using the calibration data of IntCal20 (Reimer et al., 2020). The excluded ages are written in italic.

Sample	Depth (cm)	^{14}C lab code	Material	^{14}C age (yr BP)	Calibrated ^{14}C ages (cal yr CE)	Median (cal yr CE)	Age ranges (cal yr CE)
Gahak 3-2-6	6–7	Poz-118150	Peat	127.63 ± 0.37 pMC	1970.5 ± 9	1971	11961-1980 (95%)
Gahak 3-2-38	38–39	Poz-118149	Peat	240 ± 30	1699 ± 85	1663	1526-1804 (92%)
Gahak 3-2-49	49–50	Poz-104459	Peat	405 ± 30	1498 ± 56	1475	1436-1624 (95%)
Gahak 3-2-71	*71–72*	*Aix-14049.1.1*	*Macrocharcoal*	*770 ± 100*	*1231 ± 182*	*1240*	*1040-1396 (95%)*
Gahak 3-2-74	72–74	Poz-104458	Organic mud	715 ± 30	1294 ± 33	1285	1260-1386 (95%)
Gahak 3-2-76	76–77	Poz-154221	Organic mud	945 ± 30	1100 ± 41	1101	1027-1166 (95%)
Gahak 3-2-83	83–84	Poz-154222	Organic mud	965 ± 30	1094 ± 41	1095	1024-1159 (95%)
Gahak 3-2-90	*90–91*	*Poz-118148*	*Organic mud*	*550 ± 30*	*1381 ± 37*	*1399*	*1318-1434 (95%)*

3.4. Palynological sample preparation

A total of 24 subsamples for pollen analysis were taken every 5 cm along the 120 cm core, each containing one to two cm^3. Samples were prepared for pollen and Non-Pollen Palynomorphs (NPPs) analysis using standard extraction technique (Moore et al., 1991). Pollen identifications were assisted using pollen atlases of Europe and the Mediterranean (Reille, 1992, 1995, 1998; Beug, 2004; van Zeist and Bottema, 1977) and the Pollen Reference Collection of Persia and Arabia hosted at IMBE (Aix-en-Provence, France). NPP identifications were assisted by a number of publications (Van Geel and Aptroot, 2006; Cugny, 2011; Shumilovskikh and van Geel, 2020, among others). Pollen percentages of terrestrial plants were calculated using the sum of the pollen of upland herbs, trees, and shrubs (AP + NAP) excluding aquatics/subaquatics. The reason of the exclusion of the aquatic/subaquatics was the predominance of these pollen in some samples and very low pollen production of upland steppes both masking the visibility of the upland pollen variations. Pollen percentages of aquatic plants were however, calculated based on the sum of all pollen (AP + NAP + aquatics/subaquatics). The distinction between the above ecological categories was based on both botanical literature and our field observations. Non-Pollen Palynomorphs (NPPs) (and *Triticum*-type pollen) were quantified as concentrations (true number of objects per cm^3 of sediment). To calculate pollen and NPP concentrations, *Lycopodium* tablets (Batch no. 1030, University of Lund) were added to samples and the formula presented by Stockmarr (1971) was used. Pollen percentages and NPP concentrations diagrams were created in Tilia/TGView (Grimm, 2004/2005).

3.5. Fossil insects

The whole core was cut into 10-cm thick slices for extraction of fossil

insect remains. The fossil insect extraction was performed following the method recommended by Coope (1986). In summary, samples were wet-sieved at 300 μm mesh, the residues were floated on paraffin and sorted under a binocular microscope at low magnification. The insect remains were then preserved in alcohol or glued to cardboard pieces. Taxonomic identifications were made by direct comparison with modern specimens of a reference collection. Definition of the ecological groups of the fossil coleopteran assemblages is based on the modern literature, mainly on Koch (1989a,b, 1992).

3.6. Statistical analyses

A constrained sum-of-squares cluster analysis (CONISS; Grimm, 1987) was used with the Rioja R package (Juggins, 2022) to identify zones in the stratigraphy for XRF elemental abundances and entomological data. The significance of each zone was tested with the broken stick model (Bennett, 1996) which revealed seven significant zones. However, we slightly modified the CONISS modeled zonation and reduced the number of zones from seven to five by taking into account the downcore variations of elements and their geochemical response to various environmental conditions. CONISS analysis for pollen and NPP diagrams was performed using the 'coniss' program included in Tilia/TGView (Grimm, 1987). We refer to pollen zones by "P-" and to NPP zones by "NPP-" (e.g. P-A1 & NPP-A1 zones).

In order to compare data with other regional palaeoclimate records, a Loess smoothing procedure (Local Polynomial Regression) was applied between age and each variable such as Ti XRF intensity data from Gahak (this study) and Neor (Sharifi et al., 2015) as well as $\delta^{18}O$ from Gejkar (Flohr et al., 2017). The smoothing parameter is equal to 0.05 which represents the proportion of observations used to local regression. Loess smoothing procedure (Cleveland et al., 1992) was performed in R.

And finally, a one-way non parametric ANOVA of Kruskal-Wallis and related Post Hoc test, the Conover's all-pairs test (Conover and Iman, 1979), was performed on Ti intensity variations, sum of farming-associated pollen, and pastoral pollen indicators. The objective was to test differences between the main time intervals represented in Gahak record: the Mediaeval Warm Period, the Little Ice Age, and the two episodes pre-dating and post-dating these phases. Results are classically represented with box-plot and letters that summarize significant differences or similarities between groups per periods.

3.7. Spectral and wavelet analysis

To track the degree of coherence between elemental pairs from the XRF measurements as a function of time, wavelet semblance analyses were performed based on the continuous wavelet transform method (Cooper and Cowan, 2008) using a modified MATLAB script. Time series were detrended by subtracting the least-square best-fit line from the original data using the built-in MATLAB command. Furthermore, time series were linearly interpolated at an equally spaced time step prior to the analysis.

Dominant periodicities within an unevenly spaced time series were identified by utilizing the Lomb-Scargle periodogram (Lomb, 1976; Scargle, 1982) approach using PAST software (Hammer et al., 2001) version 3.22. Prior to the analysis, the data was detrended using the built-in MATLAB command.

4. Results and interpretation

4.1. Sedimentary facies

Based on sediment textural properties, four sedimentological units can be recognized (Fig. 4). The lowest sedimentary unit (S-U1: 120-94 cm depth) is a massive gray clay with no visible layering and very few organic debris and pale mottling. It seems to show a seasonally-inundated topographic depression marking the 'pre-wetland environment'. The unit is overlaid by a 22-cm gray organic mud layer, containing a significant amount of siliciclastic minerals (S-U2: 94-71 cm depth). The organic mud layer is composed of lacustrine carbonate mud and contains intact aquatic snail shells and ostracods and is rich in plant debris. It indicates the deposition in a low-energy shallow wetland to lake environment and corresponds to the 'wetland formation phase'. The organic mud layer gradually changes into a carbonate mud with white color and without significant fossil content. This sedimentary unit (S-U3: 71-57 cm depth) is most probably deposited in an oligotrophic freshwater shallow water body and marks a phase of 'lake formation' (S-U4: 57 cm depth to the top of the section). The upper part of the core from 58 cm to the surface comprises a fibrous peat accumulation that contains a sandy peat layer around the depth of 10 cm. The contact with S-U3 is sharp and shows an abrupt change in hydrological conditions.

4.2. Radiocarbon chronology and age-depth model

Results of the eight radiocarbon dates and their associated uncertainties are presented in Table 1.

The age-depth model was generated based on smoothing spline regression (Fig. 4). We also generated an age-depth model based on Bayesian inference (not shown here), as we have previously demonstrated the effectiveness of such age models in identifying age outliers in anthropogenically disturbed small wetlands in semi-arid Iran (Djamali et al., 2021). The Bchron Bayesian model (Parnell et al., 2008) automatically excluded the age of 1381 ± 37 cal yr CE at 91-90 cm depth, which we also excluded from the clam smooth-spline model (highlighted in red in Fig. 4). In the absence of radiocarbon ages (due to the lack of organic sediment) for the lower 40 cm of the core, we retained the down-core extrapolation based on the linear regression model proposed by clam. The robustness of the record (e.g. between 85 and 65 cm depth) is presented as the age uncertainties, shown by the gray-filled curve, to the left of the proxy panels (Fig. 5 and Figs. 8–10). One of the sources of error in the age-depth modeling is the possible offset of measured ^{14}C ages from true ages due to a "reservoir effect" caused by dissolved inorganic and organic carbon (Jull et al., 2013; Zhou et al., 2022; Brisset et al., 2019). Brisset et al. (2019), showed that charcoal particles extracted from lake sediments in the limestone-dominated catchment areas of Zagros give the most reliable radiocarbon age estimates and help to overcome the problem of "reservoir effect". In order to estimate the age offset due to the reservoir effect, we were able to extract sufficient amount of charcoals from a sample collected from approximately the middle of the core at the depth of 71–72 cm. We used the AixMICADAS system at CEREGE, which is equipped with an elemental analyzer coupled to the CO_2 gaz ion source capable of handling very small samples (Bard et al., 2015; Tuna et al., 2018). The measured age is 770 ± 100 yr BP, which agrees with the nearby age of 715 ± 30 yr BP measured on bulk organic mud suggesting that the "reservoir effect" is minimal. Due to the low carbon amount (13 μg) of the charcoal-like material, the analytical error of this age is large (100 yr) and the exact nature of the dated material remains uncertain (it has a proper $\delta^{13}C$ value of −24.9 ‰ vs PDB but a low carbon proportion of 10%). This age was thus not included in the age-depth model even if it fully agrees with it.

4.3. Elemental proxies

The sedimentary profile against down-core variations in IRM field values and XRF-based relative abundance of a selection of elements including Si, Ti, Fe, K, Ca, Sr, and elemental ratios (Zr + Rb)/Sr and Si/Ca are illustrated in Fig. 5. High (Zr + Rb)/Sr and Si/Ca ratios reflect the balance between clastic and carbonate components and high values of Si/Ca typically reflect coarse grained siliciclastic terrigenous intervals (Dypvik and Harris, 2001; Lo et al., 2017). The vertical scale is based on depth with corresponding calibrated radiocarbon ages marked for each 5 cm depth intervals (both in BP and CE).

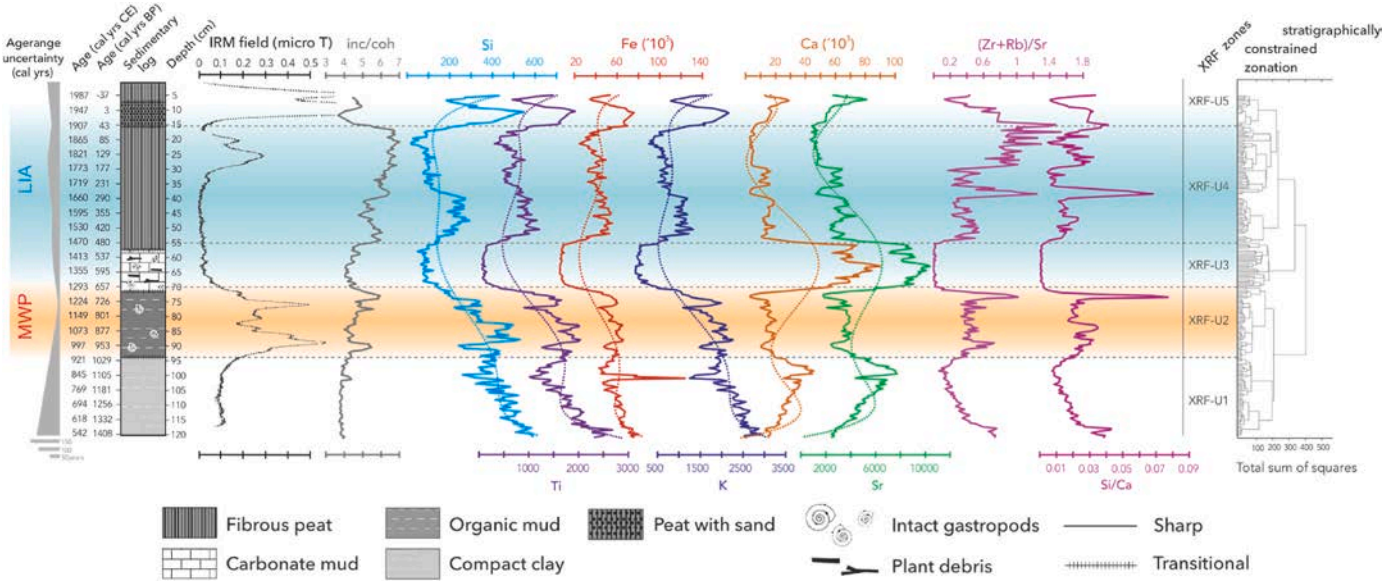

Fig. 5. Down-core XRF records of elemental abundances (XRF intensity) for detrital elements (Si, K, Fe, Rb and Ti), carbonate-related elements (Ca and Sr) and some elemental ratios. The dotted lines in the first six panels represent the 6-degree polynomial trend line. The inc/coh ratio is plotted to the left as a proxy for relative organic content (peat) in sediment. Sedimentary log and magnetic field (IRM) are also plotted to compare to XRF elemental variations.

Several episodes of enhanced elemental intensities were identified along the core. Overall, the XRF zones obtained through stratigraphically-constrained zonation (SCZ) show a good correlation with major sedimentary units. The abundances of detrital elements (Si, K, Fe, Rb and Ti) show down-core covariations. The correlation is inverse between Ca and Sr intensities from the beginning of the record at 480 CE to 1470 CE. The correlation between selected element pairs is also evident in the cross-wavelet transform (CWT) analyses (Fig. 6A–D) and their corresponding semblance wavelet analysis. These correlations suggest a single mechanism for Ti, Si, Fe, and K input to the Gahak wetland.

XRF-U1 (Depth: 120-94 cm/**Age:** 542–920 CE**): Pre-wetland environment.** Throughout this unit, the refractory lithogenic elements (Si and Ti) show a decreasing trend while Ca and Sr abundances show increasing values (Fig. 5). The unit is completely fit with the lowest sedimentary unit (S-U1), comprising massive gray clay possibly deposited in a poorly drained floodplain.

XRF-U2 (Depth: 94-70 cm/**Age:** 920–1260 CE**): Wetland formation and first erosion events**. This unit corresponds to the organic mud sedimentary unit. The ferromagnetic minerals (see IRM curve) show significantly high values with two remarkable peaks centered around 76 and 90 cm depth (960 and 1200 CE). These peaks can be interpreted as evidence of intensive and rapid soil erosion events that could be related to agro-pastoral events based on a correlation with pollen and NPP evidence of agro-pastoralism (see the interpretation of bioindicators in the next sections).

XRF-U3 (Depth: 70-55 cm/**Age:** 1260–1470 CE**): Lake formation**. The unit corresponds to a lacustrine facies. The sediment is composed of lacustrine carbonate mud rich in plant debris and aquatic snail shells and ostracods. The transition of the XRF-U2 to XRF-U3 unit is very sharp and reflected in almost all element intensity curves well seen in down-core variation in elemental z-scores Fig. S1). Ca and Sr abundances attain their highest values in the entire record. Carbonates and calcium-rich rocks are frequently available for weathering in the catchment basin of the Gahak wetland (Fig. 2A). It seems that carbonate deposition happened through biogenic mediation and/or concentration through evaporation (Gierlowski-Kordesch, 2010).

XRF-U4 (Depth: 55–15 cm/Age: 1470–1910 CE**): Peat accumulation.** The lake environment is replaced with a peat bog during the transition of XRF-U3 to XRF-U4. The peat would have lasted for the rest of the record until today. The peat formation and accumulation are recorded by inc/coh curve (Fig. 5) even if inc/coh value is not a direct indicator of organic matter (Chawchai et al., 2016). The upper part of the unit XRF-U4 is characterized by a significant peak of IRM magnetic field centered around 1750 CE and major peaks of Si/Ca and (Zr + Rb)/Sr values around 1640 CE and after 1750 CE. These peaks are related to significant inputs of coarser grained siliciclastic terrigenous materials to the wetland.

XRF-U5 (Depth: 15–0 cm/Age: 1910–1987 CE**): Anthropogenic disturbance of the peat.** The unit is characterized by extremely high IRM magnetic field values related to high content of eroded siliciclastic sands which can visually be observed intercalated in the fibrous peat. Our interpretation of anthropogenic origin for this erosion event is based on palynological evidence (please refer to Section 4.4), suggesting significant human pressure (overgrazing) on the surrounding vegetation. Accordingly, intensity of all lithogenic elements shows peaks in this unit. A decline in Si/Ca and (Zr + Rb)/Sr ratios potentially suggests that terrigenous input was dominated by fine grained particles.

Dominant periodicities in the Gahak elemental ratio (Zr + Rb)/Sr, using the Lomb-Scargle periodogram (Lomb, 1976; Scargle, 1982), revealed several periodicities centered around 220, 98, 63, 48, and 22 yrs BP (Fig. 7). The 220-year periodicity aligns well with the Suess/de Vries cycle, which corresponds to 190 to 230-year solar excursions (Steinhilber et al., 2012; Ma and Vaquero, 2020). The 98-year periodicity is close to the 84- to 92-year Gleissberg cycle (Peristykh and Damon, 2003). Peristykh and Damon (2003) also confirmed that the Gleissberg cycle is modulated by the 208-year Suess/de Vries cycle, which is reflected in their combination tones, including the ~61-year cycle. They also identified a well-resolved 44.9-year periodicity as the second harmonic of the 84- to 92-year Gleissberg cycle. These cycles are close to the 63-year and 48-year periodicities observed in the Gahak record. Finally, the 22-year periodicity corresponds to the sunspot activity cycle caused by a 22-year magnetic dynamo cycle known as Hale Cycle (Mursula et al., 2002). The correlation between the results of the spectral analysis on Gahak record and well-known solar cycles suggests that the climate of uplands of the central Iranian plateau is highly sensitive to the variations in solar irradiance.

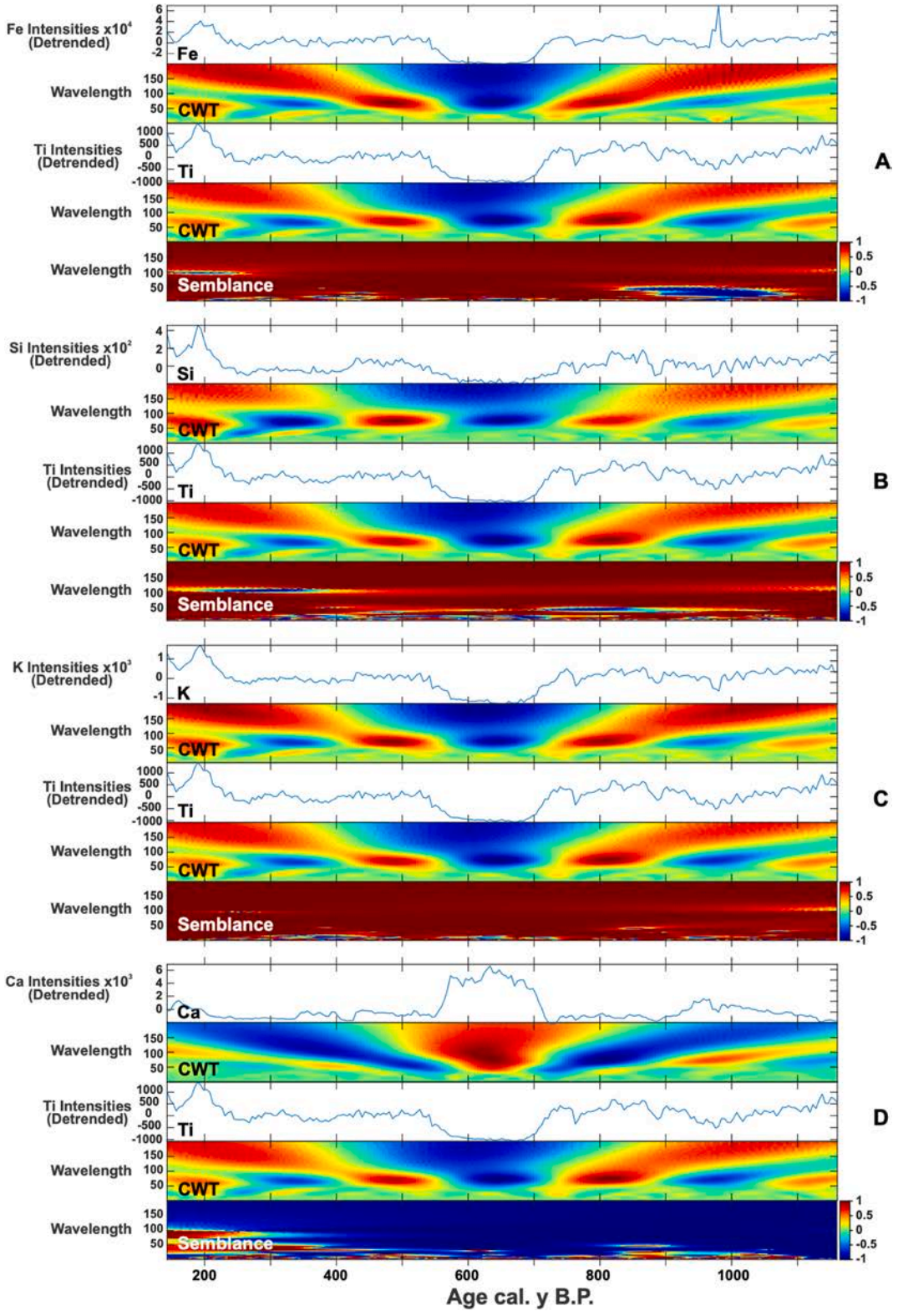

Fig. 6. Cross-wavelet transform (CWT) for elemental pairs (A–D) and their corresponding semblance wavelet analysis capture covariations in elemental abundances over time (note that in Fig. 5, the XRF records are plotted by depth). Red areas in the CWT panels indicate positive amplitude, while dark blue indicates negative amplitude. In the panels referring to semblance analysis, the degree of correlation between the relative abundances of two elements is shown in red, corresponding to a semblance of +1 (positive correlation), cyan for a semblance of zero, and dark blue for a semblance of −1 (negative or inverse correlation). For most of the record, the relative abundances of refractory and mobile elements show significant agreement (+1), except for calcium (Ca), which shows an inverse correlation. These correlations suggest a single source of elemental input to the Gahak wetland. However, the correlation between Ca and Ti is disrupted at some point after 300 years before present. (For interpretation of the references to color in this figure legend, the reader is referred to the Web version of this article.)

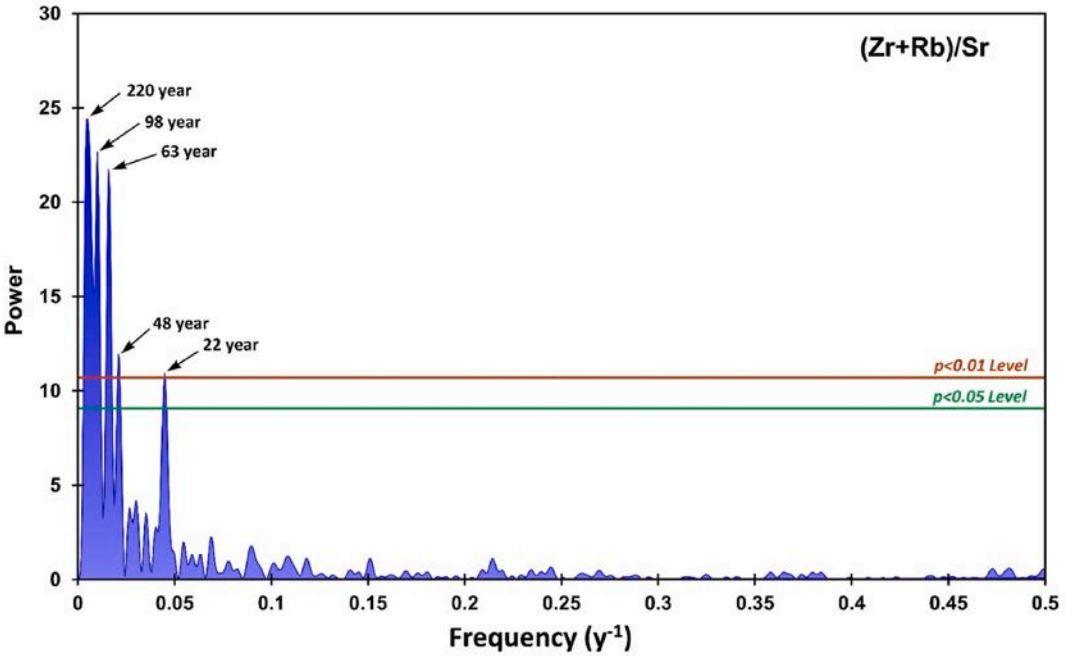

Fig. 7. Lomb-Scargle periodogram for Gahak using downcore XRF (Zr + Rb)/Sr ratios.

4.4. Pollen and non-pollen palynomorphs (NPPs)

In total, 80 pollen taxa and 17 NPP types were identified, counted, and transformed into percentages and concentrations (grains per cm^3), respectively. A simplified percentage pollen diagram with major pollen taxa attributed to different ecological groups, is illustrated in Fig. 8. NPP concentrations and their ecological groups are also illustrated in Fig. 9. Stratigraphically-confined vertical zonation schemes of both diagrams are remarkably similar and suggest almost the same subdivision of pollen and NPP records. Although, the broken stick test suggests three major zones for each diagram, we defined five major zones by giving special importance to some key pollen and NPP indicators (e.g. *Triticum*).

All pollen spectra show the predominance of an open landscape (tree percentages remaining constantly under 10%). *Quercus* (oak) pollen has a continuous curve but displays the background values reflecting the Zagros deciduous forest in western Iran (based on our unpublished data from modern pollen traps of Kashan). Traces of cultivated trees in lower elevations (*Juglans* and *Platanus*) and desert shrubs (*Calligonum* group: *Calligonum* and *Pteropyrum* spp.) growing in central Iranian plateau are also observed. Overall, pollen assemblage composition suggests an Irano-Turanian montane steppe dominated by *Artemisia*, *Cousinia*, Fabaceae, and Plumbaginaceae constituted the regional vegetation during the last millennium (Djamali et al., 2012). However, the subtle changes in relative abundance of herbaceous pollen and particularly those pollen and NPPs associated with agro-pastoralism and wetland environment reveal remarkable changes in the landscape and in the anthropogenic activities.

4.4.1. P-A1/NPP-A1 (depth: 120–97 cm/age: 542–920 CE)

Pre-wetland environment. The vegetation record starts with high values of Cichorioideae and Asteroideae associated with significant amounts of Cyperaceae all suggesting a seasonally-flooded poorly-drained flat alluvial plain colonized by plants characteristics of

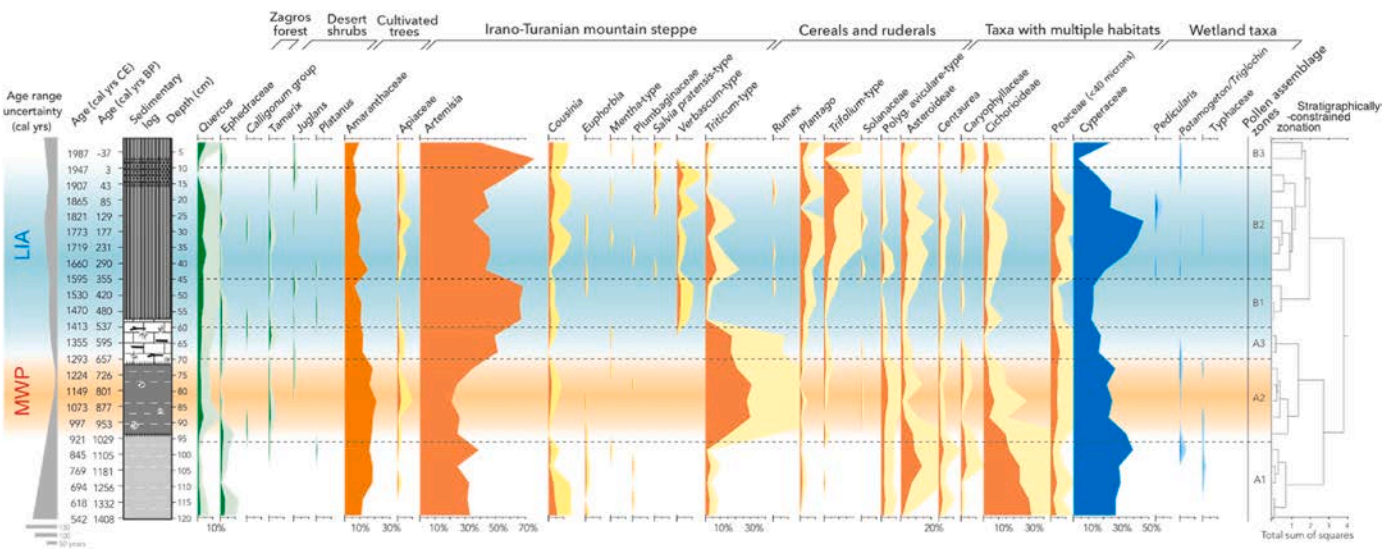

Fig. 8. Percentage diagram for a selection of pollen and spores from Gahak sediment core.

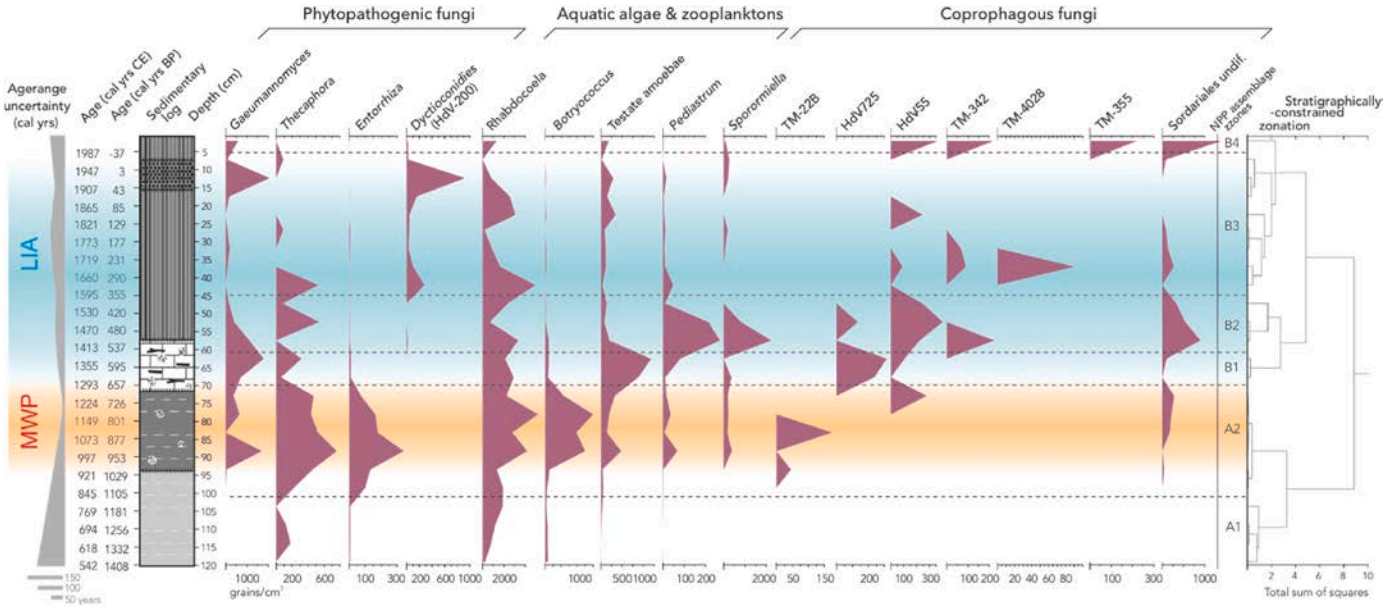

Fig. 9. Concentration diagram for 17 non-pollen palynomorphs. Concentrations are in spore numbers per cm^3 of sediment.

hydromorphic soils (zone A1). Water table may have slightly raised at the P-A1 to A2 transition (Fig. 8) as evidenced by slightly increased pollen of Typhaceae and *Potamogeton/Triglochin*. These changes accompanied with the first peak of Cyperaceae at the same transition indicate the beginning of the wetland formation also correlated with a marked change in sediments.

4.4.2. P-A2/NPP-A2 (depth: 97–72 cm/age: 920–1300 CE)

Wetland formation and establishment of a sedentary farming community. Significant amounts of Cyperaceae pollen and their associated fungi *Entorrhiza* sp., a peak of *Botryococcus*, and increasing values of *Rhabdocoela* during P-A2/NPP-A2 together suggest a permanently waterlogged ecosystem with high organic productivity. *Entorrhiza* is a genus of fungi whose species are mostly obligate parasites of Cyperaceae and Juncaceae and cause galls on root tips of these families worldwide (e.g. Bauer et al., 2015; Chater and Smith, 2018; Reiss et al., 2019).

The most spectacular feature of the Gahak pollen record is a continuous peak of *Triticum* (wheat) pollen along the P-A2 to P-A3 (NPP-A2 to B1). The identification of the wheat pollen is based on morphological criteria presented in the seminal work of Beug (2004). This was based on the pattern of the exine infra- and supratectal elements under the phase contrast (Fig. 13, page 75 in Beug, 2004) and the width of the pore, which is the largest in Cerealia-type pollen (Table 1, page 79 in Beug, 2004). Wheat pollen percentages and concentrations reach exceptionally high values exceeding 28% and 21000 grains/cm^3, respectively (Figs. 8 and 12). The almost continuous curve (although with low values) of Solanaceae and *Polygonum aviculare*-type during the same phase is noteworthy because the species of *Solanum* (i.e., *S. nigrum* and *S. villosum*) and to some extent *Polygonum aviculare* subspecies are mostly weeds in farms and gardens of most of Iran from 0 to 2400 m a.s.l. (Mosaferi et al., 2015; Eskandari et al., 2019; Eskandari and Shirzadian, 2022).

Spores of several phytopathogenic fungi also show significant peaks almost correlating with *Triticum* pollen curve (cf P-A2 to A3 with NPP-A2 to B1). Of particular interest is the almost continuous curve of the hyphopodia of *Gaeumannomyces*, a genus of sac fungi (ascomycetes) with several species well-known to cause the take-all disease infecting root system of many Poaceae and particularly the cereals (Ritz, 2005). Different former varieties of the species *Gaeumannomyces graminis* (Walker, 1972), now split into several new species including *G. graminis*, *G. avenae*, and *G. tritici* which are host-specific pathogens of cereal crops including wheat, barley, and oat (Hernàndez-Restrepo et al., 2016). *Gaeumannomyces* hyphopodia appears simultaneously with wheat cultivation strongly suggesting its association with the cereals cultivated in Gahak.

Another significant correlation of a non-pollen palynomorph with the *Triticum* curve is observed in *Thecaphora* spore curve (Fig. 9). Although we could not find any evidence of *Thecaphora* species directly infecting the wheat in modern literature, the genus belongs to a group of smut fungi commonly pathogens of cereal crops including the *Triticum* (Ram and Singh, 2004; Arias et al., 2021). *Thecaphora* species are reported as pathogens of several crops all around the world but mostly the crops originated from South America. Common examples are *T. frezii* infecting peanuts and *T. solani* infecting potato. In the Old World, most of the phytopathogenic *Thecaphora* are found in Asteraceae, Caryophyllaceae and Polygonaceae families. In Iran, *T. schwarzmaniana* has recently been reported as a pathogen of wild rhubarb species *Rheum ribes*, a wild plant used as vegetable and in traditional medicine (Vasighzadeh et al., 2014). However, unlike other pollen records of Iran e.g. that of Lake Urmia (Djamali et al., 2008), we did not find *R. ribes* pollen in the Gahak record. Similarly, *T. dahuangis* has more recently been reported to infect Chinese rhubarb *R. palmatum* (Piatek et al., 2021). The co-occurrence of *Thecaphora* curve with agricultural phase of Gahak suggests the possibility that this smut fungi was associated with a crop or crop-associated weed in the past.

4.4.3. P-A3/NPP-B1 (depth: 72–61 cm/age: 1300–1413 CE)

Decrease of cereal cultivation and formation of a lake system. The cereal cultivation continues with lower intensity during the P-A3 zone (NPP-B1) and *Artemisia* pollen starts increasing, heralding a major change in the vegetation and anthropogenic activities in Gahak which will culminate during the next pollen assemblage zone. The pollen concentration values of *Triticum* show more drastic fall compared to the pollen percentages (Figs. 8 and 12) suggesting that agricultural activities abruptly declined around 1250 CE following the most commonly accepted chronology of MWP to LIA climatic transition (e.g. Matthews and Briffa, 2005). The near absence of *Botryococcus* and lowest values of aquatic pollen, both indicate the oligotrophic conditions with lower organic productivity and substantially reduced aquatic vegetation. This is in accordance with the deposition of the lacustrine carbonate mud of S-U3 sedimentary unit (Fig. 4).

4.4.4. P-B1/NPP-B2 (depth: 61–47 cm/age: 1413–1595 CE)

Development of pastoralism and seasonal occupation of the site. During the P-B1 (NPP-B2), *Artemisia* became very important in the steppe vegetation dominating the pollen assemblages for about 160 years (Fig. 7). This remarkable *Artemisia* increase in the landscape is contemporaneous with a peak of the green algae *Pediastrum* showing an open water lacustrine environment (Fig. 9). Nowadays, *Artemisia* (*A. aucheri*) grows in well-drained soils which receive a high amount of snow-melt water during spring. Indeed, *Artemisia aucheri* currently forms a well-established community in the subalpine zone of Karkas Mountains with frequent snowfall. High amount of *Artemisia* pollen, peak of *Pediastrum*, and a lithology dominated by a lacustrine mud together suggest a significant amount of snowfall and reduced annual evapo-transpiration in Gahak environment during the period almost corresponding to the 15th-16th centuries CE (1400–1580 CE). Significant peaks of *Sporormiella* and some other dung-associated fungal spores (NPP-B2; Fig. 9) suggest a clear transition from sedentary agriculture to mobile pastoral life-style during the transition of the P-A3 to P-B1 (NPP-B1 to NPP-B2) at the very beginning of the 15th century CE.

Anthropogenic pollen indicators of pastoralism which were present with low values from the beginning of the record, start increasing from the P-B1 pollen zone until the end of the pollen diagram (Fig. 8). In the context of the Karkas Mountains, our floristic observations of high elevation montane steppes suggest that *Plantago lanceolata*-type, *Rumex*, *Verbascum*-type, *Cousinia*, and *Salvia pratensis*-type all indicate grazing activities. A significant increase in *Trifolium* pollen from the P-B1 onwards is noteworthy. The *Trifolium*-type pollen in the Gahak sequence seems identical to the pollen of the red clover (*Trifolium pratense*) widely cultivated in Eurasia as a fodder crop and has contributed to the feeding of the livestock during the seasonal occupation of the site in summer months which is still practiced nowadays. It is one of the major plants found in the wet meadows around the Gahak wetland. Combined together, both coprophilous NPPs and coprophagous beetles (see next section) are continuously present during the upper half of the Gahak sequence suggesting a continuous intensive pastoral pressure on the ecosystems in the area since the beginning of the 15th century.

4.4.5. P-B2/NPP-B3 (depth: 47- ca 5 cm/age: 1595–1947 CE)

Intensification of pastoral pressure on the montanesteppe. The pollen indicators of grazing observed in P-B1/NPP-B2, increase and form continuous curves in the P-B2 pollen zone (Fig. 8). Significant presence of coprophagous fungi corroborates the strong pastoral pressure on the steppe vegetation during the NPP-B3 subzone (Fig. 9). A peak of Cyperaceae and the presence of *Pedicularis*, suggest a densely vegetated wetland with relatively high-water tables. *Pedicularis* is currently found on the peat surface in the eastern part of the wetland. Towards the end of the subzone, a peak of the fungal cells belonging to NPP type HdV-200 correlates with a decline of Cyperaceae. The HdV-200 is mostly associated with biological decomposition of desiccated plant remains and helophytes (van Geel et al., 1989) suggesting seasonal dry conditions in Gahak at the mid-to late 19th century.

4.4.6. P-B3/NPP-B4 (depth: ca 5–0 cm/age: 1947–1987 CE)

The uppermost 5 cm of the Gahak record is particularly characterized by explosion of coprophagous fungal spores and high values of pollen indicator of grazing. *Artemisia* which currently dominates the subalpine zone of the area reaches its highest peak in the entire record. The peak of Caryophyllaceae most probably corresponds to the thorny cushion species of *Acanthophyllum* which are dominant in surrounding montane steppes. All the evidence suggests a very high pastoral pressure on the environment of the Gahak wetland during the second half of the last century.

4.5. Entomological data

31 taxa were identified based on a total of 259 fragments and 137 individuals, mostly belonging to Coleoptera (90%) with only two taxa belonging to Heteroptera and one taxon to Hymenoptera (Fig. 10). Identifications were limited to genus and family levels due to the lack of reference materials from the region. The coleopteran assemblages were relatively poor with average of 13 taxa per sample. The two lowermost samples (120-100 cm depth) were completely devoid of insect remains. The richest sample in terms of number of fragments (n = 58) was between 50 and 40 cm depth and the richest sample in terms of number of individuals (n = 26) was between 80 and 70 cm depth. The taxa were clustered under five ecological groups based on their common habitats and one group of uncertain ecological affinity; phytophagous, aquatic, riparian, coprophagous, and uncertain (Fig. 10). The grouping is based on literature (see methodology section) and our field observations. Stratigraphically-confined vertical zonation of the entomological diagram suggests two major assemblage zones referred to as Ent-A and Ent-B (Fig. 9). The lower assemblage zone Ent-A (100-50 cm: 810–1522 CE) is characterized by high abundance of both aquatic and riparian taxa and with low abundance but almost constant presence of coprophagous taxa. The upper zone Ent-B assemblage zone (50-0 cm: 1522–1952 CE) is characterized by lower abundance of aquatic and riparian taxa but higher abundance and more continuous presence of phytophagous and coprophagous taxa.

The absence of insect remains in the lower 20 cm of the core suggest less water-logged conditions and/or more frequent subaerial exposure of the site causing the decaying of the fossil materials. This part corresponds to the pre-wetland phase of the site revealed in pollen and NPP diagrams. For the rest of the diagram, aquatic and riparian taxa are mostly present indicating that the wetland and water-logged conditions have existed at least since 800 CE. Continuous presence of abundant remains of aquatic beetle genera *Ochthebius* and *Enochrus* (Fig. 11) further suggests that the Gahak wetland did not undergo complete seasonal desiccation until very recently. These permanent water-logged conditions correspond to the MWP and most of the LIA. The above beetle taxa can thus be considered as bioindicators for the seasonality of wetland's moisture or water table because they can attest to the year-round water-logged conditions.

Coprophagous taxa are present almost all along the core suggesting that pastoral activities were practiced around the Gahak wetland since the beginning of the record. The upper half of the Gahak record displays more abundant fragments and individuals of dung beetles (*Aphodius* spp. and *Onthophagus* spp.). This can be linked to two environmental factors, the taphonomic processes and changes in the intensity of grazing activities. Contrary to the lower half of the diagram in which the wetland had higher water tables, the upper half of the diagram is characterized by organic sediment build-up and by lower water-tables and/or gradual terrestrialization of the wetland. This may have made the wetland floor more accessible to the livestock grazing and direct dropping of animal dung onto the sediment surface in shallow water. More abundant dung beetles are also compatible with ever increasing values of pollen indicators of grazing (see *Plantago lanceolata*-type), nitrophilous taxa (see *Trifolium*-type pollen) and coprophilous fungal spores (Ponel et al., 2011) (Figs. 7 and 8). As far as the agricultural activities are concerned, only the presence of *Chaetocnema* sp. is noted, a genus which can occasionally be a pest of Poaceae including cereals. In the record, it is found in three intervals with cereal cultivation (compare Figs. 8 and 10).

The more noticeable occurrence of Heteroptera in the lower half of the diagram is also interesting and may indicate relatively higher temperatures. The diversity and abundance of this thermophilous group of insects would have thus increased during the Mediaeval Warm Period.

5. Discussion

5.1. MWP and LIA thermal and moisture variations reflected in Gahak record

High elevation wetlands and peat accumulations are invaluable

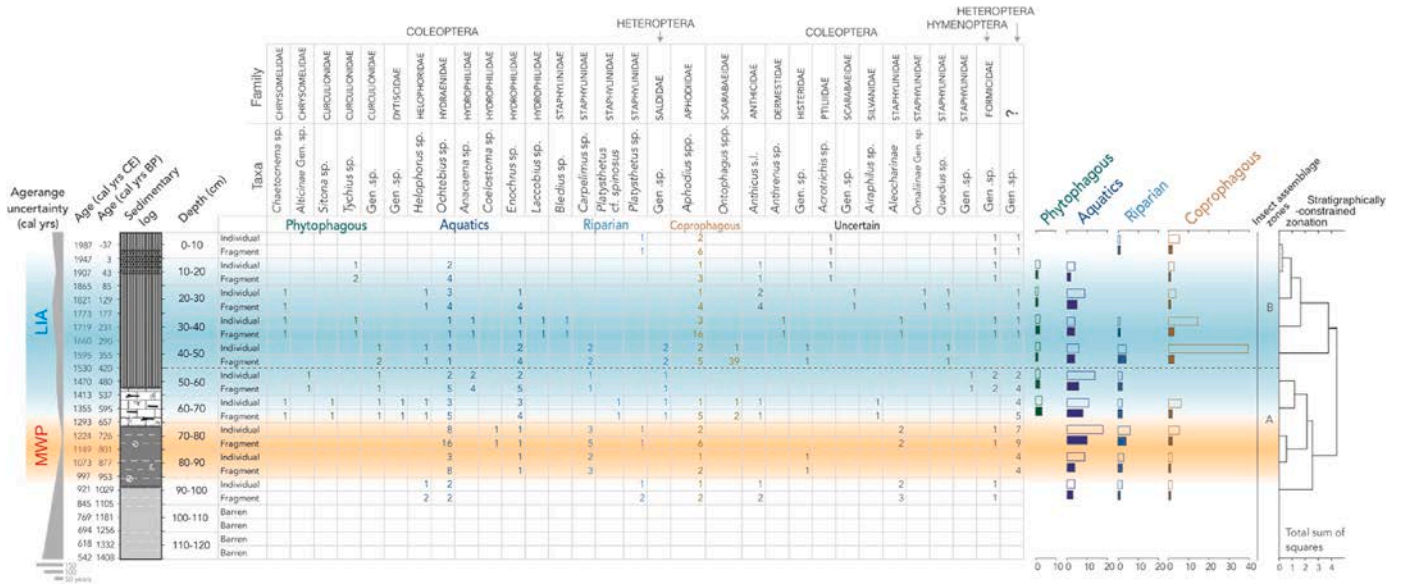

Fig. 10. Palaeoentomological record of Gahak with the number of fragments and inferred individuals for each 10-cm thick sample. Identified taxa were put into five ecological groups.

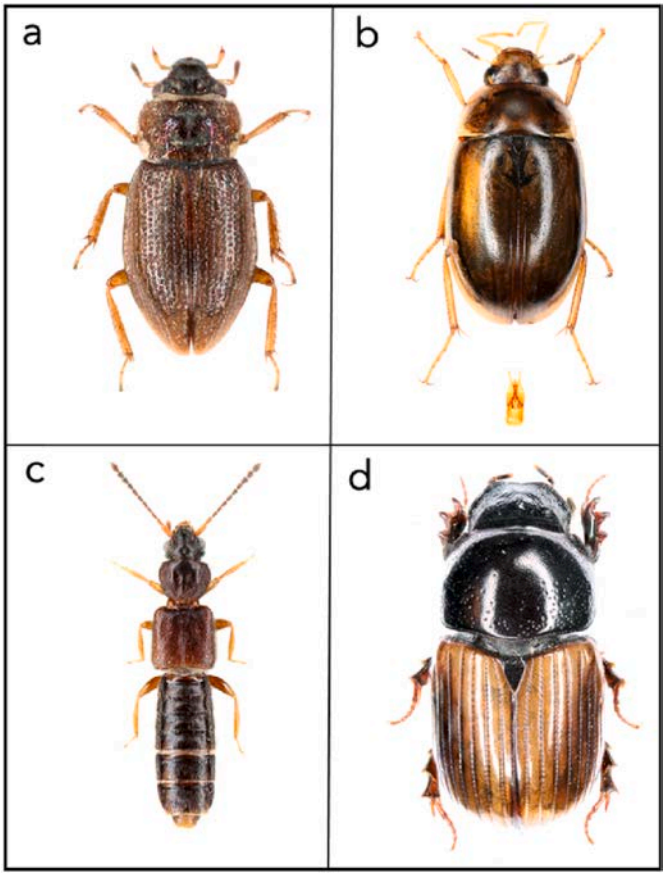

Fig. 11. Four key beetle genera frequently encountered in Gahak palaeoentomological record. a. *Ochthebius* sp. (1.7 mm long), b. *Enochrus* sp. (5.9 mm long), c. *Carpelimus* sp. (3.6 mm long), and d. *Aphodius* sp. (6 mm long). a and b are indicators of high wetland water tables with no seasonal desiccation. c is a typical riparian taxon growing on wet mud flats, and d is a dung beetle suggesting the abundance of livestock around the site.

sedimentary archives that can record changes in snow cover extension, alpine/subalpine flora and vegetation, agro-pastoral practices, and erosional events (Miehe et al., 2009; Djamali et al., 2009; Bell et al., 2021). On dry slopes of the Iranian mountains in the vicinity of desert areas, they form 'green islands' harbouring a unique plant biodiversity (Naqinezhad et al., 2009, 2021) and providing an important source of drinking water for livestock and small-scale farming activities. Gahak wetland is one of these wetlands whose multi-proxy record provides a wealth of information on the combined effects of high frequency climatic variations and anthropogenic agro-pastoral practices on wetland's hydro-sedimentary environment and surrounding montane steppes. Not only the MWP and LIA are clearly recorded in Gahak sequence but their internal fluctuations are also traceable in both bioindicator and geochemical records (Figs. 5, 8-10).

The MWP in Gahak is almost perfectly correlated with Lake Maharlou's (SW Iran) most important desiccation phase over the last four millennia (Fig. 12e; see also Brisset et al., 2019). Previously, Sharifi et al. (2015, 2018, and 2023) demonstrated how the downcore variation in Ti abundances during the Holocene can be related to the episodes of dry conditions over the interior of SW Asia. They concluded that the episodes of high Ti abundances in high-elevated Neor Lake (Sharifi et al., 2015, and 2018) are correlated to the episodes of high dust flux to the region during the dry periods. They also used lake sediment Ti/Al ratio from Lake Urmia in NW Iran along with the palaeo-rainfall reconstruction (Fig. 12g) to show the correlation between periods of low precipitation-low lake levels with the dry episodes (Sharifi et al., 2023). The high values of XRF-measured Ti intensities of Gahak (Fig. 12b) during the MWP are also well-correlated with those from Lake Neor (NW Iran) (Fig. 12c) and low precipitation values over the Lake Urmia basin (Fig. 12g) suggesting relatively warm and dry conditions or at least less effective moisture over Western Asia. These trends are in line with the sudden shift in elemental z-scores (Fig. S1) from MWP to LIA indicating a significant change in elemental input and sedimentary regime of Gahak wetland corresponding to climatic shift from MWP to LIA. This climate shift is also correlated with the variation in total solar irradiance (TSI) where the observed dry episodes in Gahak, Neor Lake and Urmia Lake during the MWP are well correlated with higher solar irradiance values (Fig. 12k). The box plots and one-way ANOVA test for the Gahak Ti intensity variations further shows the significant difference between the MWP and LIA periods. The same hydroclimatic shift is characterised by dramatic rise of the Caspian Sea levels (Fig. 12f) after a lowstand

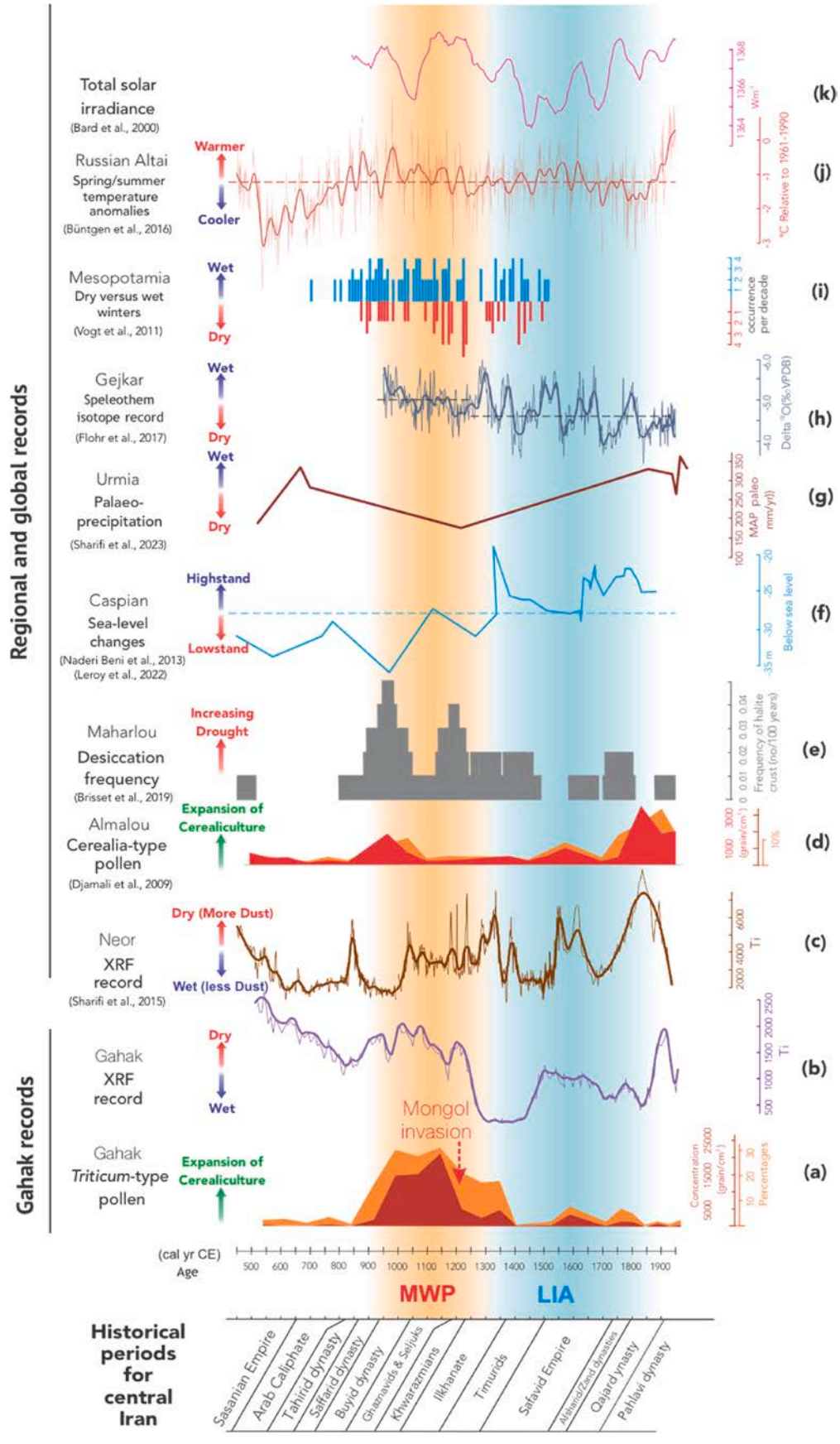

(caption on next page)

Fig. 12. The wheat cultivation phase (a) and Ti intensity variations (b) in Gahak record (this study) compared to a selection of regional and global proxy records of climate and solar activity. (c) Ti intensity variations in Lake Neor (Sharifi et al., 2015), (d) cereal pollen in Lake Almalou Djamali et al. (2009), (e) Lake Maharlou desiccation intervals (Brisset et al., 2019), (f) Caspian Sea level changes (Naderi-Beni et al., 2013; Leroy et al., 2022), (g) Lake Urmia precipitation reconstruction (Sharifi et al., 2023), (h) Oxygen isotope record of Gejkar cave in Kurdistan (Flohr et al., 2017), (i) wet and dry events in Mesopotamia (Vogt et al., 2011), (j) spring/summer temperatures based on dendro-climatological data from Russian Altai (Büntgen et al., 2016), (k) Total solar irradiance (TSI) based on cosmonuclides production record (Bard et al., 2000). The Gahak agricultural phase during the MWP correlates with a warm but relatively wet period in the Iranian plateau as suggested by frequent desiccations of the Maharlou playa lake in SW Iran (e: Brisset et al., 2019) and more negative values of $\delta^{18}O$ of speleothem records in northern Zagros (h: Flohr et al., 2017) as well as the climate historical data from Mesopotamia (i: Vogt et al., 2011).

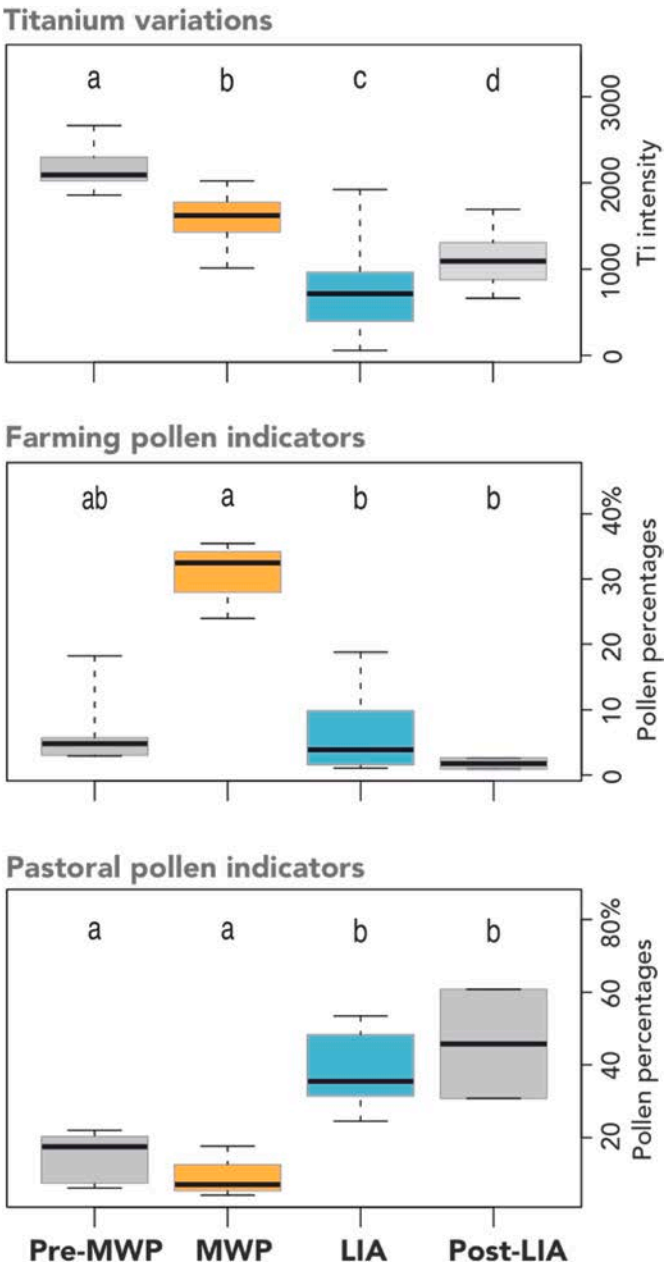

Fig. 13. Box plots for Conover's all-pairs comparison test results applied to Ti intensity variations, farming-associated pollen, and pastoral pollen indicators corresponding to four main time intervals represented in Gahak record. The one-way ANOVA (Kruskal-Wallis *H* test) shows significant differences ($p < 0.001$) between the MWP and LIA periods for all tested variables.

during the MWP (Lahijani et al., 2009; Naderi Beni et al., 2013; Leroy et al., 2022). The non-pollen palynomorphs of Almalou peat bog (NW Iran) also suggest lower wetland moisture during the MWP compared to the LIA (not shown in Fig. 12) (Djamali et al., 2009). All these correlations suggest relatively low effective moisture during the MWP in central Iran. Previous studies indicate that the interplay between the intensity of the Siberian High, the position of the mid-latitude westerly jet (MLWJ), and variations in solar irradiance potentially control precipitation patterns over Southwest Asia (Schiemann et al., 2009; Nagashima et al., 2011; Kutzbach et al., 2014). Periods of a strong Siberian High and a southward-shifted MLWJ are associated with dry and dusty conditions in interior Southwest Asia including the northern and western Iran (Sharifi et al. 2015, 2018), a pattern that persisted during the Little Ice Age (LIA). Conversely, under warmer conditions, a weaker Siberian High allows the MLWJ to migrate poleward, resulting in milder and wetter climates that are favorable for winter wheat growth. A speleothem record from northern Mesopotamia (Flohr et al., 2017) indicates a general drying trend beginning at the onset of the Medieval Warm Period (MWP). Despite this trend, the record suggests that the average effective moisture during the MWP was relatively higher and more stable compared to the Little Ice Age (LIA) (Fig. 12h). A historical climatological analysis of Arabic written sources of the Mediaeval Middle East are in line with those speleothem records and suggests wetter winters for 900–1100 CE although it shows drier winters for 1100–1250 CE (Vogt et al., 2011). It can thus be deduced that the Mediaeval Warm Period in the interior SW Asia was warm with relatively low effective moisture. However, our study shows that it was wet enough to maintain a sustainable agriculture lasting over three centuries. Indeed, almost all geochemical and biological proxies provide evidence for a permanent wetland system during the MWP even if mean water levels were lower than the onset of the LIA. Water resources were thus available to perform irrigated agriculture during the MWP. In the next section, we try to infer the MWP climatic conditions based on agro-climatological requirements of wheat.

5.2. *Mobility of agro-pastoral communities during the MWP and LIA*

The MWP has frequently been associated with a major agricultural transformation in continental Europe and the so-called 'cerealization' of northwestern Europe when the grain production was largely increased and diversified, contributing to mediaeval economic growth (Schroeder, 2023). Bread wheat (*Triticum aestivum*), rye (*Secale cereale*), and oat (*Avena sativa*), became increasingly adopted and replaced spelt wheat (*T. spelta*) and barley. In the Alps and the Mediterranean mountains, higher temperatures of the MWP permitted the establishment of permanent settlements and expansion of agricultural landscapes in higher elevations (Mensing et al., 2016; Brandolini et al., 2023). Gahak record provides undisputed evidence of a three-century long intensive cultivation of cereals and possibly other crops in the uplands of the central Iranian plateau during the Mediaeval Warm Period (Fig. 8). Due to the quasi-absence of high-resolution pollen and archaeobotanical evidence from similar high-altitude contexts of the region, it is not currently possible to generalize this farming pattern into the whole region as an indicator of the beneficial effects of the MWP climatic change for mediaeval agriculture. Nonetheless, the beginning of the MWP in a high-resolution pollen record from Lake Almalou (NW Iran; 2400 m) is also characterised by a peak of cereal cultivation although it starts decreasing earlier than the Gahak sequence at around 1100 CE (Djamali et al., 2009).

Our findings suggest that sedentary farming communities settled the area from 950 CE for more than three centuries. Fossil pollen and

entomological assemblages suggest that by the onset of the LIA, the sedentary agriculture and wheat cultivation became increasingly difficult to sustain and gave way to mobile seasonal agro-pastoralism which continues until today. This contrasted pattern of farming *versus* pastoralism during the MWP and the LIA is distinctly seen in the box plots of percentage values of anthropogenic pollen indicators (Fig. 13).

In general, the winter wheat is sown in autumn and harvested in summer of the next year. It needs moderately wet autumns, cold winters, and warm and wet springs and its yield particularly suffers from dry and cold springs and extended snow-cover, two conditions that were frequent during the LIA (Pfister and Brázdil, 2006; Pfister and Brázdil, 2006) but not during the MWP. In the highlands of the interior West Asia and Central Asia, wheat is grown as both irrigated and rain-fed grain crops with the highest percentage of dry-farmed wheat belonging to Iran in areas with mean annual precipitation exceeding 210–230 mm (Ballan and Bazin, 2012). When rain-fed, the wheat is sown in autumn to be harvested in June to October according to the elevation. When irrigated, it is also sown in autumn but will be harvested earlier from April (e.g. in lowlands of Khuzestan Province) to August. Irrigated winter bread wheat grows only on fertilized fields in rotation with summer crops (Ballan and Bazin, 2012).

Bioclimatic characteristics of the winter bread wheat, predominantly *T. aestivum*, are helpful to estimate the seasonal patterns of temperature and precipitation of Gahak mountain site during MWP and LIA. A synthesis of many experimental works has estimated that lethal minimum and maximum temperatures for winter wheat are −17.2 and 47.5 °C, and the optimal temperature range is 17–23 °C (Porter and Gawith, 1999). These agro-meteorological data on winter wheat suggest several facts on the conditions of agroecosystems of the site during both MWP and LIA. First, they suggest that during the MWP, the seasonal pattern of precipitation was different. Although the annual precipitation amount could have been lower than today, the spring was most probably warm and wet and snow-cover extension was limited. The winter temperature minima stayed above the lethal temperatures of −17.2 °C. These conditions changed dramatically at the onset of the LIA when dry and cold springs became more frequent with devastating biophysical effects on grain crops (Pfister and Brázdil, 2006). When snow cover lasts for a long time in spring, there is not enough time to sow spring wheat because the needed time for grain-filling will be too short. The LIA was thus most probably characterised by an unsuitable combination of seasonal agro-meteorological factors for both irrigated and dry cereal farming. Nowadays, the annual precipitation (213 mm in a close weather station in Abyaneh; Fig. 1) seems not sufficiently high to sustain a rain-fed wheat cultivation even if the average of minimum temperatures of coldest month (−3.9 °C) remains well above lethal temperature limit. It is thus more probable that farming communities of Gahak practiced irrigated wheat farming. The availability of water all year round in the Gahak basin as inferred by the permanent water-logged conditions, reinforces this possibility. The presence of modern qanat systems around the wetland (Fig. 2) suggests that this system could also have been used to supply irrigation water in the mediaeval time. The qanat system is an efficient groundwater exploitation system invented somewhere in the Iranian plateau and along the alluvial fans (Goblot, 1979).

The transition from MWP to LIA is clearly indicating the decline of agricultural practices at the expense of the intensification of pastoralism and grazing pressure on montane steppe ecosystems. Frequent extreme temperature events are considered as the most important factor negatively impacting the wheat yield (Porter and Gawith, 1999). Such events were definitely more frequent during the LIA (Pfister and Brázdil, 2006) and made the high elevation cereal farming unsustainable. It can naturally be concluded that sedentary farming was replaced by the nomado-pastoral lifestyle in the middle of 13th century CE in Gahak. Judging from bioindicators, the mobile seasonal agro-pastoralism with limited subsistence agriculture would have continued through the LIA until today. Small peaks of cereal cultivation centered around 1580 CE and 1725 CE (Fig. 12a), may reflect short spells of the relative climate warming during the LIA.

5.3. Historical and geopolitical context of the mediaeval warm period and Little Ice Age climatic changes in the central Iranian plateau

The agricultural expansion phase in Gahak corresponds to the reign of the Buyid, Ghaznavid, Seljuk, and Khwarazmian (or Khwarazmshahian) dynasties (Fig. 12), which successively took control of central Iran (Bosworth, 1968). The Buyid domination of the region (947–1029 CE) is particularly important because the Buyid era (934–1062 CE) marks a period of economic prosperity on the Iranian plateau (Busse, 1975). For instance, in the Fars region ('Persis') in SW Iran, large-scale hydraulic projects supported extensive agricultural activities (Saeidi Ghavi Andam et al., 2020). The Buyids, a Shi'i dynasty, gave particular favour to cities dominated by Muslim Shi'i populations, including Qum, Kashan, and surrounding areas (Amanat and Mottahedeh, 2018). Less is known about the history of the Kashan region under the Ghaznavids, who ruled from 1029 to 1051 CE. However, the region witnessed the peak of its economic prosperity during the Seljuk dynasty from 1051 CE and became a major centre for ceramic production (Amanat and Mottahedeh, 2018). At this time, increased demography and demand for food would have resulted in agricultural expansion in the highlands of Kashan and surrounding regions.

The end of the Mediaeval Warm Period agricultural phase in Gahak is remarkably well correlated with the Mongol invasion of western Asia (Fig. 12). The Mongols defeated the Khwarazmian army in 1219–1221 CE and invaded mainland Persia, including central Iran, in 1220–1240 CE (Boyle, 1968). The Mongol invasion also perfectly correlates with the beginning of the Little Ice Age. A long episode (15 years) of increased moisture and high grass productivity in central Mongolia are explained to have contributed to the formation of the political and military power that led to the Mongol invasion of Eurasia (Pederson et al., 2014). In central Iran, there seems to be no conclusive evidence on the real impact of this invasion on the socio-economy of the Kashan area (Amanat and Mottahedeh, 2018). Nevertheless, a quote from the Persian historian Zakariya al-Qazvini, dated to 1283 CE, suggests that 50 years after the arrival of the Mongols and under the Ilkhanate rule, Kashan was still maintaining its important position as a major centre for the production and transportation of utensils and vessels (quoted in Amanat and Mottahedeh, 2018, pp. 406–407). A close look at wheat pollen curves shows that while pollen percentage values start decreasing from 1200 CE, concentration values remain relatively high for the next 150 years during the Ilkhanates and early Timurids (Fig. 12). Hence, it is most probably the severe climatic conditions of the LIA that ended the MWP agricultural phase and favoured a nomadic seasonal pastoral lifestyle for the following centuries. Similar to our conclusion, a recent study suggests that the decline of Central Asian irrigation-based urban societies was more related to a long-term drought regime rather than the mere Mongol invasion and destruction of cities in 1219 (Toonen et al., 2020).

For more than two centuries (1501–1736 CE) during the Little Ice Age, central parts of Persia experienced a period of political stability under the Safavid Empire. The near absence of agricultural activities in Gahak during the Safavid era is thus more logically attributed to severe climatic conditions rather than socio-political factors. The following quote from the book entitled *History of Kashan* (mid-18th century) suggests abundant snow and névés in the Karkas Mountains west of Kashan during the last decades of the Little Ice Age (early to mid-18th century):

"The winding road leads to the quaint village of Rahagh, nestled among the Sardsir ('highland pasture') Kashan hills to the west of Kashan, eight parasangs (approximately 48 km) away from the city. Beyond the village lies a majestic mountain with numerous valleys, each boasting its own water sources, lush trees, crimson barberries, and verdant fields. The mountain is two parasangs from the village (approximately 12 km), and its lofty peak remains snow-capped for years on its right flank, while on its left side, a road descends past the

Gadok pass and joins the Wasaf river" (Zarrabi, 2000).

6. Conclusions

The alpine/subalpine wetlands of arid and semi-arid Southwest Asia are unique archives of hydroclimatic variations, ecosystem dynamics, and anthropogenic activities during the Holocene. The information obtained from these archives can be compared and contrasted with documentary and historical-climatological proxy data, especially for the pre-instrumental period. However, sources on mediaeval and pre-industrial human activities in Southwest Asian mountain areas are scarce compared to European mountain systems, highlighting the significance of sedimentary archives in uncovering the modality and intensity of these activities.

Our case study demonstrates that climatic shifts and their associated impacts on agro-pastoral practices, lifestyle changes, and the mobility of human communities have been clearly recorded in these archives. Our data suggest that the Mediaeval Warm Period would have favoured high-elevation agricultural activities, while the Little Ice Age increased seasonal agro-pastoral practices in the highlands of Southwest Asia. Such information may be missing in written sources available to historians and ethno-archaeologists. These archives can refine our understanding of the role of small farming communities living in remote mountain areas in the economy of Mediaeval Persia and surrounding regions.

Many high-elevation wetlands and their sedimentary records are threatened by overgrazing, man-made drainage for land reclamation, and erosion. It is highly recommended that conservation measures be rapidly implemented to protect these high-elevation wetlands. The sedimentary sequences of the most endangered and eroding deposits should be systematically sampled, and the sediment cores deposited and kept in appropriate natural repositories for future research.

CRediT authorship contribution statement

Morteza Djamali: Conceptualization, Methodology, Investigation, Visualization, Writing – original draft. **Emmanuel Gandouin:** Formal analysis, Software, Data curation, Visualization. **Arash Sharifi:** Methodology, Investigation, Data curation, Visualization, Writing – original draft. **Philippe Ponel:** Methodology, Investigation, Visualization, Writing – original draft. **Kazuyo Tachikawa:** Resources, Investigation, Methodology, Validation, Writing – review & editing. **Alireza Naqinezhad:** Investigation, Writing – original draft. **Abdolmajid Naderi-Beni:** Resources, Investigation, Writing – review & editing. **Hamid Lahijani:** Resources, Investigation, Writing – review & editing. **Jacques-Louis de Beaulieu:** Investigation, Validation, Supervision. **Elodie Brisset:** Visualization, Validation, Supervision. **Nafiseh Samadi:** Investigation. **Marjan Mashkour:** Validation, Supervision. **Emma Gamba:** Investigation, Writing – review & editing. **Dahvya Belkacem:** Methodology, Resources. **Michelle Leydet:** Data curation, Visualization. **Alireza Behnam:** Resources. **Marta Garcia:** Methodology, Resources. **François Demory:** Methodology, Investigation, Data curation, Writing – review & editing. **Edouard Bard:** Resources, Validation, Supervision.

Declaration of generative AI and AI-assisted technologies in the writing process

Authors declare that no Generative AI and AI-assisted technologies were used during the process of writing of this manuscript.

Declaration of competing interest

The authors declare that they have no known competing financial interests or personal relationships that could have appeared to influence the work reported in this paper.

Acknowledgement

We wish to thank Prof. Reza Mansouri (former director of the Iranian National Observatory - INO) for his encouragement and full support from the beginning of this study, and Dr. Habib Khosroshahi, the current director of INO, for continuing to support our project. Laboratory analyses and radiocarbon measurements were supported by the "PALEO-PERSEPOLIS" ANR-DFG project (2015–2019) funded by the Agence Nationale de la Recherche (ANR-14-CE35-0026-01), the LIA project entitled "HAOMA" funded by the Centre National de la Recherche Scientifique (CNRS), and the SINERGIA "MITRA" project funded by the Swiss National Science Foundation (Grant No. 10000157). Field investigations were also partly supported by the Franco-Iranian Gundishapour joint project entitled "KECO-INO" (2015–2016). We thank Frauke Rostek and Thibaut Tuna for their help with the ^{14}C measurements at CEREGE.

Appendix A. Supplementary data

Supplementary data to this article can be found online at https://doi.org/10.1016/j.quascirev.2025.109202.

Data availability

NOAA and Neotoma

References

Amanat, M., Mottahedeh, R.P., 2018. Medieval Kashan: crossroads of commerce and culture. Eurasian Stud. 16, 395–429.

Amidi, S.M., 1977. Étude géologique de la région de Natanz-Surk (Iran Central). stratigraphie et pétrologie. Geological Survey of Iran 42, 316.

Arias, S.L., Mary, V.S., Velez, P.A., Rodriguez, M.G., Otaiza-Gonzáles, S., Theumer, M.G., 2021. Where does the peanut smut pathogen, *Thecaphora frezii*, fit in the spectrum of smut diseases? Plant Dis. 105, 2268–2280.

Ballan, D., Bazin, M., 2012. Gandom. Encyclopedia Iranica 10, 270–276.

Bard, E., Raisbeck, G., You, F., Jouzel, J., 2000. Solar irradiace during the last 1200 years based o cosmogenic nuclides. Tellus B 52, 985–992.

Bard, E., Tuna, T., Fagault, Y., Bonvalot, L., Wacker, L., Fahrni, S., Synal, H.-A., 2015. AixMICADAS, the accelerator mass spectrometer dedicated to 14C recently installed in Aix-En Provence, France. Nucl. Instrum. Methods Phys. Res. B 361, 80–86.

Barlow, M., Zeitchik, B., Paz, S., Black, E., Evans, J., Hoel, A., 2016. A review of drought in the Middle East and Southwest Asia. J. Clim. 29, 8547–8574.

Bauer, R., Garnica, S., Oberwinkler, F., Reiss, K., Weiß, M., Begerow, D., 2015. Entorrhizomycota: a new fungal phylum reveals new perspectives on the evolution of fungi. PLoS One 10, e0128183.

Bayer Altin, T., Kayan, M., 2020. Climatic and social change during the little Ice age in Cappadocia vicinity, southern central anatolia, Turkey. Reg. Environ. Change 20, 16. https://doi.org/10.1007/s10113-020-01604-x.

Bell, B.A., Fletcher, W.J., Hughes, P.D., Cornelissen, H.L., Fink, D., Rhoujjati, A., 2021. Palynological evidence from a sub-alpine marsh of enhanced little Ice age snowpack in the marrakech high atlas, north Africa. Veg. Hist. Archaeobotany 31, 49–66.

Bennett, K.D., 1996. Determination of the number of zones in a biostratigraphical sequence. New Phytol. 132, 155–170.

Berberian, M., King, G.C.P., 1981. Toward a paleogeography and tectonic evolution of Iran. Can. J. Earth Sci. 18, 210–265.

Beug, H.J., 2004. Leitfaden der Pollenbestimmung für Mitteleuropa und angrenzende Gebiete. Verlag Dr Friedrich Pfeil, München.

Blaauw, M., 2010. Methods and code for "classical" age-modelling of radiocarbon sequences. Quat. Geochronol. 5, 512–518.

Bosworth, C.E., 1968. Chapter 1: the political and dynastic history of the Iranian world (A.D. 1000-1217). In: Boyle, J.A. (Ed.), The Cambridge History of Iran, Volume V: the Saljuq and Mongol Periods. Cambridge University Press, Cambridge, pp. 1–202.

Boyle, J.A., 1968. Chapter 4: Dynastic and political history of the il-Khans. In: Boyle, J.A. (Ed.), The Cambridge History of Iran, Volume V: the Saljuq and Mongol Periods. Cambridge University Press, Cambridge, pp. 303–421.

Brandolini, F., Kinnaird, T.C., Srivastava, A., Turner, S., 2023. Intensification of terrace agriculture on the northern apennines during the medieval climate anomaly. EGU General Assembly 2023, Vienna, Austria, pp. 24–28. Apr 2023, EGU23-5591.

Brisset, E., Djamali, M., Bard, E., Borschneck, D., Gandouin, E., Garcia, M., Stevens, L., Tachikawa, K., 2019. Late Holocene hydrology of Lake Maharlou, southwest Iran, inferred from high-resolution sedimentological and geochemical analyses. J. Paleolimnol. 61, 111–128.

Bronk Ramsey, C., 1995. Radiocarbon calibration and analysis of stratigraphy: the OxCal program. Radiocarbon 37, 425–430.

Büntgen, U., Myglan, V.S., Charpentier Ljugqvist, F., McCormick, M., Di, Cosmo, Sigl, M., Jungclaus, J., Wagner, S., Krusic, P.J., Esper, J., Koplan, J.O., de Vaan, M.A.,

Luterbacher, J., Wacker, L., Tegel, W., Kirdyanov, A.V., 2016. Cooling and societal change during the late antique little Ice age from 536 to around 660 AD. Nat. Geosci. 9, 231–236.
Busse, H., 1975. Chapter 7: Iran under the buyids. In: Fry, R.N. (Ed.), The Cambridge History of Iran. Volume IV: the Period from the Arab Invasion to the Saljuqs. Cambridge University Press, Cambridge, pp. 250–304.
Chater, A., Smith, P.A., 2018. Recent finds of Entorrhiza root smuts. Field Mycol. 19, 55–60.
Cleveland, W.S., Grosse, E., Shyu, W.M., 1992. Chapter 8: local regression models. In: Chambers, J.M., Hastie, T.J. (Eds.), Statistical Models in S. Routledge, New York, p. 68.
Chawchai, S., Kylander, M.E., Chabangborn, A., Löwemark, L., Wohlfarth, B., 2016. Testig commonly used X-ray fluorescence core scanning-based proxies for organic-rich lake sediments and peat. Boreas 45, 180–189.
Conover, W.J., Iman, R.L., 1979. On Multiple-Comparisons Procedures, Technical Reports LA-7677-MS. Los Alamos Scientific Laboratory, Los Alamos.
Coope, G.R., 1986. Coleoptera analysis. In: Berglund, B.E. (Ed.), Handbook of Holocene Palaeoecology and Palaeohydrology. Wiley & Sons, Chichester, pp. 703–713.
Cooper, G.R.J., Cowan, D.R., 2008. Comparing time series using wavelet-based semblance analysis. Comput. Geosci. 34, 95–102.
Croudace, I.W., Rindby, A., Rothwell, R.G., 2006. ITRAX: Description and Evaluation of a New Multi-Function X-Ray Core Scanner, vol. 267. Geological Society of London Special Publication, pp. 51–63.
Cugny, C., 2011. Apport des microfossiles non-polliniques à l'histoire du pastoralisme sur le versant nord Pyrénéen : entre référentiels actuels et reconstitution du passé, vols. 1 & 2. Unpublished PhD Dissertation, Université Toulouse 2, Le Mirail.
Del Socorro Lozano-Garcia, M., Caballero, M., Ortega, B., Rodriguez, A., Sosa, S., 2007. Tracing the effects of the little Ice age in the tropical lowlands of eastern Mesoamerica. Proc. Natl. Acad. Sci. USA 104, 16200–16203.
Demory, F., Uehara, M., Quesnel, Y., Rochette, P., Romey, C., Tachikawa, K., Garcia, M., Borschneck, D., Pignol, L., Bard, E., Andrieu-Ponel, V., 2019. A new high-resolution magnetic scanner for sedimentary sequences. G-cubed 20, 3186–3200.
Djamali, M., de Beaulieu, J.-L., Shah-Hosseini, M., Andrieu-Ponel, V., Amini, A., Akhani, H., Leroy, S.A.G., Stevens, L., Alizadeh, H., Ponel, P., Brewer, S., 2008. A late Pleistocene long pollen record from Lake Urmia, NW Iran. Quat. Res. 69, 413–420.
Dypvik, H., Harris, N.B., 2001. Geochemical facies analysis of fine-grained siliciclastics using Th/U, Zr/Rb and (Zr+Rb)/Sr ratios. Chem. Geol. 181, 131–146. https://doi.org/10.1016/S0009-2541(01)00278-9.
Djamali, M., de Beaulieu, J.-L., Miller, N., Andrieu-Ponel, V., Berberian, M., Gandouin, E., Lahijani, H., Ponel, P., Salimian, M., Guiter, F., 2009. A late Holocene pollen record from Lake Almalou in NW Iran: evidence for changing land-use in relation to some historical events during the last 3700 years. J. Archaeol. Sci. 36, 1346–1375.
Djamali, M., Akhani, H., Khoshravesh, R., Andrieu-Ponel, V., Ponel, P., Brewer, S., 2011. Application of the Global Bioclimatic Classification to Iran: implications for understanding the modern vegetation and biogeography. Ecol. Mediterr. 37, 91–114.
Djamali, M., Baumel, A., Brewer, S., Jackson, S.T., Kadereit, J.W., López-Vinyallonga, S., Mehregan, I., Shabanian, E., Simakova, A., 2012. Ecological implications of Cousinia Cass. (Asteraceae) persistence through the last two glacial-interglacial cycles in the continental Middle East for the Irano-Turanian flora. Rev. Palaeobot. Palynol. 172, 10–20.
Djamali, M., Rashidian, E., Askari-Chaverdi, A., Aubert, C., Brisset, E., Demory, F., Faucherre, N., Gandouin, E., Lahijani, H.A.K., Marriner, N., Naderi-Beni, A., Parnell, A., 2021. Early Sasanian landscape reshaping: new geoarchaeological evidence from the Ardashir Pond in southwest Iran (Palace of Ardashir, third Century CE). Geoarchaeology 36, 925–942.
Emadodin, I., Reinsch, T., Taube, F., 2019. Drought and Desertification in Iran. Hydrology 6, 66.
Eskandari, M., Assadi, M., Shirzadian, S., Mehregan, I., 2019. Ethnobotanical study and distribution of the *Solanum* section *Solanum* species (Solanaceae) in Iran. J. Med. Plants 18, 85–98.
Eskandari, M., Shirzadian, S., 2022. Introduction of Important Weeds of Solanaceae in Iran. Iranian Research Institute of Plant Protection technical report, 61382 (in Persian).
Fleitmann, D., Haldon, J., Bradley, R.S., Burns, S.J., Cheng, H., Edwards, R.L., Raible, C. C., Jacobson, M., Matter, A., 2022. Droughts and societal change: the environmental context for the emergence of Islam in late Antique Arabia. Science 376, 1317–1321.
Flohr, P., Fleitmann, D., Zorita, E., Sadekov, A., Cheng, H., Bosomworth, M., Edwards, L., Matthews, W., Matthews, R., 2017. Late Holocene droughts in the Fertile Crescent recorded in a speleothem from northern Iraq. Geophys. Res. Lett. 44, 1528–1536.
Ge, Q., Wu, W., 2011. Climate during the medieval climate anomaly in China. PAGES News 19, 24–26.
Gierlowski-Kordesch, E.H., 2010. Lacustrine carbonates. Dev. Sedimentol. 61, 1–101.
Goblot, H., 1979. Les Qanats : une technique d'acquisition de l'eau. École des hautes études en sciences sociales, Paris.
Grimm, E.C., 1987. Coniss: a Fortran 77 program for stratigraphically constrained cluster analysis by the method of incremental sum of squares. Comput. Geosci. 13, 13–35.
Grimm, E.C., 2004/2005. TILIA and TGView Software. Illinois State University, Illinois, Version 2.0.2.
Gurjazkaite, K., Routh, J., Djamali, M., Vaezi, A., Poher, Y., Naderi-Beni, A., Tavakoli, V., Kyln, H., 2018. Vegetation history and human-environment interactions through the late Holocene in Konar Sandal, SE Iran. Quat. Sci. Rev. 194, 143–155.
Haghani, S., Leroy, S.A.G., Khdir, S., Naderi Beni, A., Lahijani, H.A.K., 2015. An early 'Little Ice Age' brackish water invasion along the south coast of the Caspian Sea (sediment of Langarud wetland) and its wider impacts on environment and people. Holocene 26, 3–16.
Hassanzadeh, J., Wernicke, B.P., 2016. The Neotethyan Sanandaj-Sirjan zone of Iran as an archetype for passive margin-arc transitions. Tectonics 35, 586–621.
Hernàndez-Restrepo, M., Groenwald, J.Z., Elliott, M.L., Canning, G., McMillan, V.E., Crous, P.W., 2016. Take-all or nothing. Stud. Mycol. 83, 19–48.
Hammer, Ø., Harper, D.A.T., Ryan, P.D., 2001. PAST: paleontological statistics software package for education and data analysis. Palaeontol. Electron. 4.
Hua, Q., Turnbull, J.C., Santos, G.M., Rakowski, A.Z., Ancapichun, S., De pol-Holz, R., Hammer, S., Lehman, S.J., Levi, I., Miller, J.B., Palmer, J.G., Turney, C.S.M., 2022. Atmospheric radiocarbon for the period 1950-2019. Radiocarbon 64, 723–745.
Hughes, P.D., 2014. Little Ice age glaciers in the mediterranean mountains. Méditerranée 122, 63–79.
Isfahani, F., Sharifi, A., 1999. Geochemical Characteristics of Magmatic Rocks of Iran. Geological Survey of Iran, Treatise on Geology of Iran, vol. 2. Book No. 70.
Juggins, S., 2022. Rioja: analysis of quaternary science data. R package version (1.0–5). https://cran.r-project.org/package=rioja.
Jones, M.D., Djamali, M., Holmes, J., Weeks, L., Leng, M.J., Lashkari, A., Alamdari, K., Noorollahi, D., Thomas, L., Metcalfe, S.E., 2015. Human impact on the hydroenvironment of Lake Parishan, SW Iran, through the late-Holocene. Holocene 25, 1651–1661.
Jull, A., Burr, G., Hodgins, G., 2013. Radiocarbon dating, reservoir effects, and calibration. Quat. Int. 299, 64–71.
Kjær, K.H., Bjork, A.A., Kjeldsen, K.K., Hansen, E.S., Andresen, C.S., Siggaard-Andersen, M.-L., Shfaqat, A., Khan, e, Anne Sofie Søndergaard, f, Colgan, W., Schomacker, A., Woodroffe, S., Funder, S., Rouillard, A., Jensen, J.F., Larsen, N.K., 2022. Glacier response to the little Ice age during the neoglacial cooling in Greenland. Earth Sci. Rev. 227, 103984.
Koch, K., 1989a. Die Kafer Mitteleuropas, Okologie 1. Krefeld: Goecke and Evers.
Koch, K., 1989b. Die Kafer Mitteleuropas, Okologie 2. Krefeld: Goecke and Evers.
Koch, K., 1992. Die Kafer Mitteleuropas, Okologie 3. Krefeld: Goecke and Evers.
Koch, J., Clague, J.J., 2011. Extensive glaciers in northwest North America during Medieval time. Climatic Change 107, 593–613.
Koch, J., 2015. Little Ice Age and recent glacier advances in the Cordillera Darwin, Tierra del Fuego, Chile. Anales Instituto Patagonia 43, 127–136.
Kroonenberg, S.B., Abdurakhmanov, G.M., Badyukova, E.N., van der Borg, K., Kalashnikov, A., Kasimov, N.S., Rychagov, G.I., Svitoch, A.A., Vonhof, H.B., Wesselingh, F.P., 2007. Solar-forced 2600 BP and little Ice age highstands of the Caspian Sea. Quat. Int. 173–174, 137–143.
Kutzbach, J.E., Chen, G., Cheng, H., Edwards, R.L., Liu, Z., 2014. Potential role of winter rainfall in explaining increased moisture in the Mediterranean and Middle East during periods of maximum orbitally-forced insolation seasonality. Clim. Dynam. 42, 1079–1095.
Lahijani, H.A.K., Rahimpour-Bonab, H., Tavakoli, V., Hosseindoost, M., 2009. Evidence for late Holocene highstands in central Guilan-East Mazandaran, south Caspian coast, Iran. Quat. Int. 197, 55–71.
Leroy, S.A.G., Lahijani, H., Djamali, M., Vahabi-Moghadam, Naqinezhad, A., Shah-Hosseini, M., Miller, C.S., Tavakoli, V., 2011. Late little Ice age palaeoenvironmental records from the Anzali and Amirkola Lagoons (south Caspian Sea): vegetation and Sea level changes. Palaeogeogr. Palaeoclimatol. Palaeoecol. 302, 415–434.
Leroy, S.A.G., Reimer, P.J., Lahijani, H.K.A., Naderi Beni, A., Sauer, E., Chalié, F., Arpe, K., Demory, F., Mertens, K., Belkacem, D., Kakroodi, A.A., Omrani Rekavandi, H., Nokandeh, J., Amini, A., 2022. Caspian Sea levels over the last 2200 years, with new data from the SE corner. Geomorphology 403, 108136.
Lo, F.L., Chen, H.F., Fang, J.N., 2017. Discussion of suitable chemical weathering proxies in sediments by comparing the dissolution rates of minerals in different rocks. J. Geol. 125, 83–99.
Lomb, N.R., 1976. Least-squares frequency analysis of unequally spaced data. Astrophys. Space Sci. 39, 447–462.
Ma, L., Vaquero, J.M., 2020. New evidence of the Suess/de Vries cycle existing in historical naked-eye observations of sunspots. Open Astron 29, 28–31.
Magnan, G., van Bellen, S., Davies, L., Froese, D., Garneau, M., Mullan-Boudreau, G., Zaccone, C., Shotyk, W., 2018. Impact of the Little Ice Age cooling and 20th century climate change on peatland vegetation dynamics in central and northern Alberta using a multi-proxy approach and high-resolution peat chronologies. Quat. Sci. Rev. 185, 230–243.
Moore, P.D., Webb, J.A., Collinson, M.E., 1991. Pollen Analysis, second ed. Blackwell, Oxford.
Matthews, J.A., Briffa, K.R., 2005. The 'Little Ice Age': re-evaluation of an evolving concept. Geographiska Annaler 87A, 17–36.
McGregor, H., Evans, M., Goosse, H., et al., 2015. Robust global ocean cooling trend for the pre-industrial Common Era. Nat. Geosci. 8, 671–677.
Mensing, S., Tunno, I., Cifani, G., Passigli, S., Noble, P., Archer, C., Piovesan, G., 2016. Human and climatically induced environmental change in the Mediterranean during the Medieval climate anomaly and little Ice age: a case from central Italy. Anthropocene 15, 49–59.
Miehe, G., Miehe, S., Kaiser, K., Reudenbach, C., Behrendes, L., Duo, L., Schlütz, F., 2009. How old is pastoralism in Tibet? An ecological approach to the making of a Tibetan landscape. Palaeogeogr. Palaeoclimatol. Palaeoecol. 276, 130–147.
Mosaferi, S., Sheidai, M., Keshavarzi, M., Noormohammadi, Z., 2015. *Polygonum aviculare* (Polygonaceae) subspecies, new records for the flora of Iran. Mod. Phytomorphol. 8, 31–36.
Mursula, K., Usoskin, I.G., Kovaltsov, G.A., 2002. A 22-year cycle in sunspot activity. Advan. Space Res. 29, 1979–1984.

Nagashima, K., Tada, R., Tani, A., Sun, Y., Isozaki, Y., Toyoda, S., Hasegawa, H., 2011. Millennial-scale oscillations of the westerly jet path during the last glacial period. J. Asian Earth Sci. 40, 1214–1220.
Naqinezhad, A., Jalili, A., Attar, F., Ghahreman, A., Wheeler, B.D., Hodgson, J.G., Shaw, S.C., Maassoumi, A.A., 2009. Floristic characteristics of the wetland sites on dry southern slopes of the Alborz Mts., N. Iran: the role of altitude in floristic composition. Flora 204, 254–269.
Naderi Beni, A., Lahijani, H., Mousavi Harami, R., Arpe, K., Leroy, S.A.G., Marriner, N., Berberian, M., Andrieu-Ponel, V., Djamali, M., Mahboubi, A., Reimer, P.J., 2013. Caspian sea-level changes during the last millennium: historical and geological evidence from the south Caspian Sea. Clim. Past 9, 1645–1665.
Naqinezhad, A., Nowak, A., Świerszcz, S., Jalili, A., Kamrani, A., Wheeler, B.D., et al., 2021. Syntaxonomy and biogeography of the Irano-Turanian mires and springs. Appl. Veg. Sci. 24, e12571.
Oglesby, R.J., Feng, S., Hu, Q., Rowe, C., 2011. Medieval drought in north America: the role of the Atlantic multidecadal oscillation. PAGES News 19, 18–20.
PAGES2k Consortium, 2017. A global multiproxy database for temperature reconstructions of the Common Era. Sci. Data 4, 170088.
Parnell, A.C., Haslett, J., Allen, J.R.M., Buck, C.E., Huntley, B., 2008. A flexible approach to assessing synchroneity of past events using Bayesian reconstructions of sedimentation history. Quat. Sci. Rev. 27, 1872–1885.
Pederson, N., Hessl, A.E., Baatarbileg, N., Anchukaitis, K.J., Di Cosmi, N., 2014. Pluvials, droughts, the Mongol empire, and modern Mongolia. Proc. Natl. Acad. Sci. USA 111, 4375–4379.
Peregrine, P.N., 2020. Climate and social change at the start of the late antique little Ice age. Holocene 30, 1643–1648.
Peristykh, A.N., Damon, P.E., 2003. Persistence of the Gleissberg 88-year solar cycle over the last ~12,000 years Evidence from cosmogenic isotopes. J. Geophys. Res.: Space Phys. 108, 1–15.
Pfister, C., 1981. An analysis of the Little Ice Age climate in Switzerland and its consequences for agricultural production. In: Wigley, T.M.L., Ingram, M.J., Farmer, G. (Eds.), Climate and History: Studies in Past Climates and Their Impact on Man. Cambridge University Press, Cambridge, pp. 214–248.
Pfister, C., Brázdil, R., 2006. Social vulnerability to climate change in the "Little Ice Age": an example from Central Europe in the early 1770's. Clim. Past 2, 115–129.
Piatek, M., Lutz, M., Wang, Y., Wang, S., Kellner, R., 2021. *Thecaphora dahuangis*, a new species causing leaf smut disease of the traditional medicinal plant *dahuang (Rheum palmatum)* in China. Plant Pathol. 70, 1292–1299.
Ponel, P., Court-Picon, M., Badura, M., Guiter, F., Beaulieu, J.-L. de, Andrieu-Ponel, V., Djamali, M., Leydet, M., Gandouin, E., Buttler, A., 2011. Holocene history of Lac des Lauzons (2180 m a.s.l.), reconstructed from multiproxy analyses of Coleoptera, plant macro-remains and pollen (Hautes-Alpes, France). Holocene 21, 565–582.
Porter, J.R., Gawith, M., 1999. Temperatures and the growth and development of wheat: a review. Eur. J. Agron. 10, 23–36.
Quinn, J.A., 2009. Desert Biomes. Greenwood Press, Westport.
Radfar, J., 1993. 1:100.000 Geological Map of Kashan. Geological Survey of Iran.
Ram, B., Singh, K.P., 2004. Smuts of wheat: a review. Indian Phytopathol. 57, 125–134.
Ramezani, E., Marvie Mohadjer, M.R., Knapp, H.-D., Ahmadi, H., Joosten, H., 2008. The late-Holocene vegetation history of the Central Caspian (Hyrcanian) forests of northern Iran. Holocene 18, 305–319.
Ramezani, E., 2013. Palynological reconstruction of late-Holocene vegetation, climate, and human impact in Kelardasht (Mazandaran province, N Iran). Iran. J. Forest Poplar Res. 21, 48–62.
Rashidian, E., Djamali, M., 2023. Landscape change and settlement dynamics in prehistory and late antiquity in the Firuzabad plain (south fars, Iran); a preliminary. J. Archaeol. Sci.Rep 47, 103805.
Reille, M., 1992. Pollen et spores d'Europe et d'Afrique du Nord. Laboratoire de botanique historique et de palynologie, Marseille.
Reille, M., 1995. Pollen et spores d'Europe et d'Afrique du Nord, vol. 1. Laboratoire de botanique historique et de palynologie-Supplément, Marseille.
Reille, M., 1998. Pollen et spores d'Europe et d'Afrique du Nord, vol. 2. Laboratoire de botanique historique et de palynologie-Supplément, Marseille.
Reimer, P., Austin, W., Bard, E., Bayliss, A., Blackwell, P., Bronk Ramsey, C., Butzin, M., Cheng, H., Edwards, R., Friedrich, M., Grootes, P., Guilderson, T., Hajdas, I., Heaton, T., Hogg, A., Hughen, K., Kromer, B., Manning, S., Muscheler, R., et al., 2020. The IntCal20 northern hemisphere radiocarbon age calibration curve (0–55 cal kBP). Radiocarbon 62, 725–757.
Reiss, K., Schön, M.E., Ziegler, R.R., Lutz, M., Shivas, R.G., Piatek, M., Garnica, S., 2019. The origin and diversification of the Entorrhizales: deep evolutionary roots but recent speciation with phylogenetic and phylotypic split between associates of the Cyperaceae and Juncaceae. Org. Divers. Evol. 19, 13–30.
Ritz, K., 2005. Fungi. In: Hillel, D. (Ed.), Encyclopedia of Soils in the Environment, pp. 110–119.
Rowan, A.V., 2017. The 'Little Ice Age' in the Himalaya: a review of glacier advance driven by Northern Hemisphere temperature change. Holocene 27, 292–308.
Scargle, J.D., 1982. Studies in astronomical time series analysis. II - statistical aspects of spectral analysis of unevenly spaced data. Astrophys. J. 263, 835–853.
Schroeder, N., 2023. The 'Cerealization' of continental north-west Europe, *c.* 800-1200. In: Hamerow, H., McKerracher, M. (Eds.), New Perspectives on the Medieval Agricultural Revolution; Crop, Stock and Furrow. Liverpool University Press, Liverpool, pp. 199–210.
Saeidi Ghavi Andam, S., Djamali, M., Nelle, O., Naderi Beni, A., Haghighifard, M., Brisset, E., Poschlod, P., 2020. Vegetation history of the Maharlou basin (SW Iran) with special reference to the Achaemenid period (550-330 BC). Veg. Hist. Archaeobotany 30, 595–610.
Schiemann, R., Lüthi, D., Schär, C., 2009. Seasonality and interannual variability of the westerly jet in the Tibetan Plateau region. J. Clim. 22, 2940–2957.
Sharifi, A., Pourmand, A., Canel, E.A., Ferer-Tyler, E., Peterson, L.C., Aichner, B., Feakins, S.J., Daryaee, T., Djamali, M., Naderi Beni, A., Lahijani, H.A.K., Swart, P.K., 2015. Abrupt climate variability since the last deglaciation based on a high-resolution, multi-proxy peat record from NW Iran: the hand that rocked the Cradle of Civilization? Quat. Sci. Rev. 123, 215–230.
Sharifi, A., Murphy, L.N., Pourmand, A., Clement, A.C., Canuel, E.A., Naderi Beni, A.A.K., Lahijani, H., Delanghe, D., Ahmady-Birgani, H., 2018. Early-Holocene greening of the Afro-Asian dust belt changed sources of mineral dust in West Asia. Earth Planet Sci. Lett. 481, 30–40.
Sharifi, A., Djamali, M., Peterson, L.C., Swart, P.K., Guadolupe Pulido Ávila, M., Esfahainejad, M., de Beaulieu, J.-L., Lahijani, H.A.K., Pourmand, A., 2023. The rise and demise of Iran's Urmia Lake during the Holocene and the anthropocene: "what's past is prologue". Reg. Environ. Change 23, 121. https://doi.org/10.1007/s10113-023-02119-x.
Shumilovskikh, L.S., van Geel, B., 2020. Non-pollen palynomorphs. In: Henry, A.G. (Ed.), Handbook for the Analysis of Micro-particles in Archaeological Samples. Springer, pp. 65–94.
Steinhilber, F., Abreu, J a, Beer, J., Brunner, I., Christl, M., Fischer, H., Heikkliä, U., Kubik, P.W., Mann, M., McCracken, K.G., Miller, H., Miyahara, H., Oerter, H., Wilhelms, F., 2012. 9,400 Years of cosmic radiation and solar activity from Ice cores and tree rings. In: Proceedings of the National Academy of Science of the USA, pp. 5967–5971.
Stöcklin, J., 1968. Structural History and Tectonics of Iran: a Review, vol. 52. The American Association of Petroleum Geologist Bulletin, pp. 1229–1258.
Stockmarr, J., 1971. Tablets with spores used in absolute pollen analysis. Pollen Spores 13, 615–621.
Thomson, M.J., MacDonald, G.M., 2020. Climate and growing season variability impacted the intensity and distribution of Fremont maize farmers during and after the Medieval Climate Anomaly based on a statistically downscaled climate model. Environ. Res. Lett. 15, 105002.
Toonen, W.H.J., Macklin, M.G., Dawkes, Giles, Durcan, J.A., Leman, M., Nikolayev, Y., Yegorov, A., 2020. A hydromorphic reevaluation of the forgotten river civilizations of Central Asia. In: Proceedings of the National Academy of Sciences, vol. 117, pp. 32982–32988.
Tuna, T., Fagault, Y., Bonvalot, L., Capano, C., Bard, E., 2018. Development of small CO_2 gas measurements with AixMICADAS. Nucl. Instrum. Methods Phys. Res. B 437, 93–97.
Vaezi, A., Routh, J., Djamali, M., Tavakoli, V., Naderi Beni, A., Roberts, P., 2022. New multi-proxy record shows potential impacts of precipitation on the rise and ebb of Bronze Age and Imperial Persian societies in southeastern Iran. Quat. Sci. Rev. 298, 107855.
Van Geel, B., Coope, G.R., van der Hammen, T., 1989. Palaeoecology and stratigraphy of the Lateglacial type section at Usselo (The Netherlands). Rev. Palaeobot. Palynol. 60, 25–129.
Van Geel, B., Aptroot, A., 2006. Fossil ascomcycetes in Quaternary deposits. Nova Hedwigia 89, 313–329.
Van Zeist, W., Bottema, S., 1977. Palynological investigations in western Iran. Palaeohistoria 19, 19–85.
Vasighzadeh, A., Zafari, D., Selcuk, F., Huseyin, E., Kursat, M., Lutz, M., Piatek, M., 2014. Discovery of *Thecaphora schwarzmaniana* on *Rheum ribes* in Iran and Turkey: implications for the diversity and phylog- eny of leaf smuts on rhubarbs. Mycol. Prog. 13, 881–892.
Vogt, S., Glaser, R., Luterbacher, J., Riemann, D., Al Dyab, Gh, Schoenbein, J., Garcia-Bustmante, E., 2011. PAGES 19, 28–29.
Waldinger, M., 2022. Medieval Warm Period (MWP) and little Ice age (LIA). J. Polit. Econ. 130, 2275–2314.
Walker, J., 1972. Type studies on Gaeumannomyces graminis and related fungi. Trans. Br. Mycol. Soc. 58, 427–457.
Zarrabi, A.K., 2000. Tarikh I Kashan (The History of Kashan), Amir Kabir, Tehran (in Persian).
Zhou, W., Chui, Y., Yang, L., Cheng, P., Chen, N., Ming, G., Hu, Y., Li, W., Lu, X., 2022. ^{14}C geochronology and radiocarbon reservoir effect of reviewed lakes studies in China. Radiocarbon 64, 833–844.